YITP-SB-20-18

Putting SMEFT Fits to Work

Sally Dawson[1],[*] Samuel Homiller[2],[†] and Samuel D. Lane[1,3‡]

[1]*Department of Physics, Brookhaven National Laboratory, Upton, New York 11973 U.S.A.*

[2]*C. N. Yang Institute for Theoretical Physics, Stony Brook University, Stony Brook, New York 11794 U.S.A.*

[3]*Department of Physics and Astronomy, University of Kansas, Lawrence, Kansas, 66045 U.S.A*

arXiv:2007.01296v3 [hep-ph] 26 Apr 2021

Abstract

The Standard Model Effective Field Theory (SMEFT) provides a consistent framework for comparing precision measurements at the LHC to the Standard Model. The observation of statistically significant non-zero SMEFT coefficients would correspond to physics beyond the Standard Model (BSM) of some sort. A more difficult question to answer is what, if any, detailed information about the nature of the underlying high scale model can be obtained from these measurements. In this work, we consider the patterns of SMEFT operators present in five example models and discuss the assumptions inherent in using global fits to make BSM conclusions. We find that including renormalization group effects has a significant impact on the interpretation of the results. As a by-product of our study, we present an up-dated global fit to SMEFT coefficients in the Warsaw basis including some next-to-leading order QCD corrections in the SMEFT theory.

[*]Electronic address: dawson@bnl.gov

[†]Electronic address: samuel.homiller@stonybrook.edu

[‡]Electronic address: samuel.lane@ku.edu

Contents

I. Introduction 3

II. Matching Models to the SMEFT 4

A. Matching Procedure and Renormalization Group 5

B. Models 9

C. Summary of Models 12

III. Results 13

A. Methodology 13

B. Model Dependent Results 15

1. Singlet Model 15

2. 2HDM 17

3. Heavy Colored particles in Loops: T VLQ 20

4. Heavy Colored particles in Loops: $(T\,B)$ VLQ 22

C. Global Fit to SMEFT Coefficients 24

IV. Discussion 26

Acknowledgments 28

A. Additional Details on the Models 28

1. Singlet Scalar 28

2. A Second Higgs Doublet 29

3. Colored Extensions of the SM 31

a. SU(3) Triplet $SU(2)_L$ Singlet Fermion 31

b. SU(3) Triplet $SU(2)_L$ Doublet Fermion 33

c. SU(3) Triplet Scalar 35

References 36

I. INTRODUCTION

With the Higgs discovery in hand and the Standard Model (SM) field content complete, one of the primary goals of the LHC is to make precise measurements of SM processes, with the hope of testing its limitations. As the search for new particles has been unsuccessful as yet, much attention has shifted towards precision measurements of Higgs processes. In this direction, the SMEFT (SM effective field theory) framework becomes very useful. In the SMEFT, deviations from the SM are parameterized by a tower of $SU(3)\times SU(2)_L\times U(1)_Y$ invariant higher dimension operators containing only SM fields. The SMEFT is useful because it provides a consistent, gauge-invariant theoretical interpretation of the data, in which higher order corrections can be included, and connects Higgs data with electroweak precision observables at the Z and W poles, diboson data, and top quark measurements. There have been numerous global fits to LHC and LEP data, yielding limits on the allowed values of the SMEFT coefficients [1–5], but thus far all of these fits are totally consistent with the Standard Model, further demonstrating the robustness of the SM.

Ultimately, however, one hopes that the SMEFT is parameterizing some high scale physics beyond the Standard Model (BSM), and it is of interest to understand how these global fits should be interpreted in this context. The goal of this work is to consider just such an interpretation in detail for a set of simple benchmark models. We consider a sample set of UV complete models where the BSM physics contains particles at mass scales above the weak scale, $\Lambda \gg M_Z$. Each model makes a prediction for the SMEFT coefficients at the high scale, $C_i(\Lambda)$, and typically only a small subset of dimension-6 operators are generated [6–8]. As we will see, all of our models predict particular relationships between the different coefficients generated, and we will explore the differences in fitting with these particular patterns as opposed to general values of the coefficients. We will mostly restrict ourselves to tree-level matching between the BSM physics and the SMEFT at the scale Λ, but we will also consider the renormalization group running to evolve the coefficients at leading logarithm to the weak scale [9, 10], where the predictions can be compared with fits to the data. Since many of our benchmark models generate operators that are well constrained by electroweak precision observables, including these leading logarithmic effects will significantly change the interpretations of the fits. These considerations are an important first step in understanding what we can learn about possible

UV complete models, and, if a deviation from the Standard Model is observed, how we can discriminate between them. This goal is sometimes referred to as the "Higgs Inverse Problem".

Understanding the sensitivity to BSM physics through the extraction of SMEFT coefficients is also useful for comparing the reach of future accelerators [11] and our calculations are part of an extended effort to understand the complementarity of the direct observation of new particles with precision measurements [12]. In addition to Higgs signal strength data, we include theory predictions with NLO QCD corrections for VV and VH ($V = W, Z$) production [13], and the leading logarithmic NLO QCD and electroweak corrections to Z and W pole observables computed in the full SMEFT [14]. As a by-product of our study, we obtain an update of the global fit to SMEFT coefficients in the Warsaw basis.

We begin by describing how we match our benchmark models to the SMEFT, including the effects of renormalization group evolution (RGE) of the Wilson coefficients down to the weak scale. We then summarize each of the models in turn in Section II B. The operators generated in each model are summarized in Section II C. We then perform a series of fits customized for each model in Section III, and discuss how the SMEFT fit results can differ depending on the correlations present in the underlying high scale model. Here we will further emphasize the role of the renormalization group evolution of the coefficients in the interpretation of SMEFT fit results. Finally, we conclude with our updated global fit in Section III C and a discussion of future directions in this type of study in Section IV.

II. MATCHING MODELS TO THE SMEFT

In this section, we lay out our benchmark models, and tabulate the relevant SMEFT coefficients obtained in the decoupling limit of these models. The models are chosen to be simple but representative BSM models with new particles at the $\sim$ few TeV scale with only a small set of unknown parameters. The full set of dimension-6 operators that we will consider, ignoring flavor, is given in Table I.

$\mathcal{O}_{ll}$	$(\bar{l}_L\gamma_\mu l_L)(\bar{l}_L\gamma^\mu l)_L$	$\mathcal{O}_{HWB}$	$(H^\dagger\tau^a H)\, W^a_{\mu\nu}B^{\mu\nu}$	$\mathcal{O}_{HD}$	$\left(H^\dagger D^\mu H\right)^*\left(H^\dagger D_\mu H\right)$
$\mathcal{O}_{He}$	$(H^\dagger i\overleftrightarrow{D}_\mu H)(\bar{e}_R\gamma^\mu e_R)$	$\mathcal{O}_{Hu}$	$(H^\dagger i\overleftrightarrow{D}_\mu H)(\bar{u}_R\gamma^\mu u_R)$	$\mathcal{O}_{Hd}$	$(H^\dagger i\overleftrightarrow{D}_\mu H)(\bar{d}_R\gamma^\mu d_R)$
$\mathcal{O}^{(3)}_{Hq}$	$(H^\dagger i\overleftrightarrow{D}^a_\mu H)(\bar{q}_L\tau^a\gamma^\mu q_L)$	$\mathcal{O}^{(1)}_{Hq}$	$(H^\dagger i\overleftrightarrow{D}_\mu H)(\bar{q}_L\gamma^\mu q_L)$	$\mathcal{O}^{(3)}_{Hl}$	$(H^\dagger i\overleftrightarrow{D}^a_\mu H)(\bar{l}_L\tau^a\gamma^\mu l_L)$
$\mathcal{O}^{(1)}_{Hl}$	$(H^\dagger i\overleftrightarrow{D}_\mu H)(\bar{l}_L\gamma^\mu l_L)$	$\mathcal{O}_{H\Box}$	$(H^\dagger H)\Box(H^\dagger H)$	$\mathcal{O}_{eH}$	$(H^\dagger H)\bar{l}_L\tilde{H}e_R$
$\mathcal{O}_{HG}$	$(H^\dagger H)G^A_{\mu\nu}G^{\mu\nu,A}$	$\mathcal{O}_{uH}$	$(H^\dagger H)(\bar{q}_L\tilde{H}u_R)$	$\mathcal{O}_{dH}$	$(H^\dagger H)(\bar{q}_L H d_R)$
$\mathcal{O}_{HB}$	$(H^\dagger H)B_{\mu\nu}B^{\mu\nu}$	$\mathcal{O}_{HW}$	$(H^\dagger H)W^a_{\mu\nu}W^{\mu\nu,a}$	$\mathcal{O}_W$	$\epsilon_{abc}W^{\nu,a}_\mu W^{\rho,b}_\nu W^{\mu,c}_\rho$
$\mathcal{O}_H$	$(H^\dagger H)^3$				

,

TABLE I: Dimension-6 operators in the Warsaw basis that are considered in this study. The fermion labels u, d, e refer generically to all 3 generations and similarly for the quark, q, and lepton, l, doublets.

A. Matching Procedure and Renormalization Group

Here we lay out our benchmark models, and tabulate the relevant SMEFT coefficients obtained in the decoupling limits of the models. The models are chosen to be well studied BSM models with new particles at the UV scale and are quite simple models, involving a small set of unknown parameters. We assume that the new particles are at a high mass scale and integrate them out of the theory using the equations of motion at tree level, although for future studies it would be of interest to perform the matching at one-loop, since one-loop matching typically generates a much richer spectrum of SMEFT operators than does the tree level matching [7, 15, 16]. This procedure generates predictions for SMEFT coefficients at the mass scale Λ corresponding to the new physics,

$$\mathcal{L} = \mathcal{L}_{SM} + \sum_i \frac{C_i}{\Lambda^2}\mathcal{O}^6_i + \dots\,, \tag{1}$$

where we include the dimension-6 operators in the Warsaw basis [17, 18]. The operators consist of all of the $SU(3)\times SU(2)_L\times U(1)_Y$ operators that can be constructed from SM fields. Since we assume $\Lambda \gg M_Z$, we only consider the dimension-6 operators, O^6_i. Some of the models we consider generate effects only for third generation quarks, so we do not

always assume flavor universality in the quark sector. The importance of the assumptions about flavor in the results of the global fits has been emphasized in Refs. [2, 19].

We fit data from Higgs processes, diboson WW and WZ production, and electroweak precision observables (EWPOs), including the W mass and width, to the patterns of SMEFT coefficients generated in our examples. For completeness, we define the operators appearing in this work in Table I and we neglect flavor indices in this table, although we will include them in some of the models. We define H to be the $SU(2)_L$ doublet Higgs field with neutral component $\frac{h+v}{\sqrt{2}}$ and, in terms of the first generation, $q_L^T = (u_L, d_L)$, $l_L^T = (\nu_L, e_L)$. Our notation follows that of Ref. [17].

At tree level, the Z and W pole observables depend on,

$$\mathcal{O}_{ll}, \quad \mathcal{O}_{HWB}, \quad \mathcal{O}_{HD}, \quad \mathcal{O}_{He}, \quad \mathcal{O}_{Hd}, \quad \mathcal{O}_{Hu}, \mathcal{O}_{Hq}^{(3)}, \quad \mathcal{O}_{Hq}^{(1)}, \quad \mathcal{O}_{Hl}^{(3)}, \quad \mathcal{O}_{Hl}^{(1)}, \tag{2}$$

and the EWPOs are sensitive to eight combinations of these operators [14, 20–22], (at NLO they are sensitive to a combination of 10 operators). We also include the $2-$ loop contribution to M_W generated by $\mathcal{O}_H$ [23, 24].

We consider tree level contributions from the following operators to Higgs data,

$$\begin{aligned} &\mathcal{O}_{HW}, \quad \mathcal{O}_{HB}, \quad \mathcal{O}_{HWB}, \quad \mathcal{O}_{HD}, \quad \mathcal{O}_{HG}, \quad \mathcal{O}_{H\Box}, \quad \mathcal{O}_{Hl}^{(3)}, \quad \mathcal{O}_{He}, \\ &\mathcal{O}_{Hu}, \quad \mathcal{O}_{Hd}, \quad \mathcal{O}_{ll}, \quad \mathcal{O}_{Hq}^{(1)}, \quad \mathcal{O}_{Hq}^{(3)}, \quad \mathcal{O}_{eH}, \quad \mathcal{O}_{uH}, \quad \mathcal{O}_{dH}\,. \end{aligned} \tag{3}$$

We also include the loop contributions to Higgs production and decay from $\mathcal{O}_H$ [25–27].

Finally, the diboson WW and WZ data depend on 7 effective couplings[1], which involve the operators

$$\mathcal{O}_{HWB}, \quad \mathcal{O}_{HD}, \quad \mathcal{O}_{W}, \quad \mathcal{O}_{Hl}^{(3)}, \quad \mathcal{O}_{ll}, \quad \mathcal{O}_{Hq}^{(1)}, \quad \mathcal{O}_{Hq}^{(3)}, \quad \mathcal{O}_{Hu}, \quad \mathcal{O}_{Hd}, \tag{4}$$

for a total of 19 operators involved in our study when we neglect flavor. For the vector-like quark models we consider, only contributions to operators involving third generation quark interactions are generated. Most of the operators that contribute to the global fits that we list above do not arise in the models we consider and we comment on the importance of this in the concluding discussion.

[1] See [28] for a convenient mapping from the effective interactions to the Warsaw basis.

The models we consider are chosen to illustrate various types of new physics and to demonstrate uncertainties and assumptions that are made when forming physics conclusions from the global fits. The models fall in two categories.

- Models with high scale scalar resonances: We consider a real scalar singlet model, both with and without a Z_2 symmetry, and a 2 Higgs doublet model (2HDM) in the decoupling limit.

- Models with new particles in loops: We consider two models with vector-like quarks (VLQs): One with a color triplet fermion with charge $Q = \frac{2}{3}$, and one with a color triplet, $SU(2)_L$ doublet of quarks with charge $Q = (\frac{2}{3}, -\frac{1}{3})$. We also briefly compare the results of the models with vector-like quarks with a model containing a heavy color triplet scalar.

There have been extensive studies in the literature computing SMEFT coefficients in these models. We summarize the models we consider below and the reader is referred to the original literature for further details.

The fits are performed in two different manners. In the first approach, we match the coefficients at the UV scale Λ to the model predictions and perform the global fit. These fits are only sensitive to the ratios $\frac{C_i}{\Lambda^2}$ and give no independent information about the UV scale. We always make the identification that Λ is the mass of the heavy particle that has been integrated out. In the second set of fits, we match the coefficients to the model predictions at Λ and then use the renormalization group to evolve the coefficients to M_Z before performing the fits. The coefficients at the weak scale are then,

$$C_i(M_Z) = C_i(\Lambda) - \frac{1}{16\pi^2}\dot{C}_i \log\left(\frac{\Lambda}{M_Z}\right), \ \dot{C}_i \equiv \gamma_{ij} C_j \,. \tag{5}$$

A complete set of the relevant anomalous dimensions in the Warsaw basis is in Refs. [29–31]. In many cases, the RGE has a dramatic effect on the interpretation of the fits. The EWPO and diboson data place strong constraints on $\mathcal{O}_{HD}$, $\mathcal{O}_{H\Box}$, and $\mathcal{O}_{HWB}$. The contributions involving the first and second generation quarks to $\mathcal{O}^{(3)}_{Hq}$, and $\mathcal{O}^{(1)}_{Hq}$ are strongly constrained by Higgstrahlung data, while the $Z \to b\bar{b}$ data constrain these operators with 3^{rd} generation quarks. In models where these coefficients are generated by RGE (even when they are not present at the matching scale), the constraints and the interpretations change dramatically [10].

To illustrate the importance of including the RGE when fitting to UV complete models, we consider the strongly constrained operators, $\mathcal{O}_{HD}$, $\mathcal{O}_{H\Box}$, $\mathcal{O}_{Hq}^{(1)}$ and $\mathcal{O}_{Hq}^{(3)}$ [13]. $\mathcal{O}_{HD}$ is not generated at tree level in any of the models we consider, while $\mathcal{O}_{H\Box}$ arises at tree level in the singlet model. Including only contributions from terms that are generated at tree level in the models we consider (see Table II),

$$
\begin{aligned}
\dot{C}_{HD} &= \frac{8}{3}g'^{\,2}\left[2C_{Ht} - C_{Hb} + \left(C_{Hq}^{(1)}\right)_{33}\right] + \frac{20}{3}g'^{\,2}C_{H\Box} \\
&\quad -24\left[Y_t^2 C_{Ht} - Y_b^2 C_{Hb} + Y_b Y_t C_{Htb}\right] \\
&\quad +24\left(Y_t^2 - Y_b^2\right)\left(C_{Hq}^{(1)}\right)_{33} \\
\dot{C}_{H\Box} &= 6g^2\left(C_{Hq}^{(3)}\right)_{33} + \frac{2}{3}g'^{\,2}\left[2C_{Ht} - C_{Hb} + \left(C_{Hq}^{(1)}\right)_{33}\right] \\
&\quad +\left[-\frac{4}{3}g'^{\,2} - 4g^2 + 12\left(Y_t^2 + Y_b^2\right) + 4Y_\tau^2\right]C_{H\Box} \\
&\quad -6\left[(Y_b^2 - Y_t^2)\left(C_{Hq}^{(1)}\right)_{33} + 3(Y_b^2 + Y_t^2)\left(C_{Hq}^{(3)}\right)_{33} + Y_t^2 C_{Ht} - Y_b^2 C_{Hb} - 2Y_b Y_t C_{Htb}\right]
\end{aligned}
$$

$$
\begin{aligned}
\left(\dot{C}_{Hq}^{(3)}\right)_{33} &= 3\left[Y_b^2 - Y_t^2\right]\left(C_{Hq}^{(1)}\right)_{33} + \left[-\frac{11}{3}g^2 + 8Y_t^2 + 8Y_b^2 + 2Y_\tau^2\right]\left(C_{Hq}^{(3)}\right)_{33} \\
&\quad -\frac{1}{6}\left[3Y_t^2 + 3Y_b^2 - g^2\right]C_{H\Box} \\
\left(\dot{C}_{Hq}^{(1)}\right)_{33} &= \left[\frac{5}{9}g'^{\,2} + 10Y_t^2 + 10Y_b^2 + 2Y_\tau^2\right]\left(C_{Hq}^{(1)}\right)_{33} - 9\left[Y_t^2 - Y_b^2\right]\left(C_{Hq}^{(3)}\right)_{33} \\
&\quad -\frac{1}{2}\left[\frac{g'^{\,2}}{9} + Y_b^2 - Y_t^2\right]C_{H\Box} - (Y_t^2 + \frac{4}{9}g'^{\,2})C_{Ht} - (Y_b^2 + \frac{2}{9}g'^{\,2})C_{Hb}\,, \qquad (6)
\end{aligned}
$$

where $C_{Ht}, C_{Hb}, C_{Htb}, C_{H\tau}, (C_{Hq}^{(1)})_{33}$ and $(C_{Hq}^{(3)})_{33}$ correspond to operators including only the third generation fermions. See [29–31] for a full expression. We note that $\mathcal{O}_{HD}$ arises from the RGE in the (TB) VLQ model and in the singlet model, and so we expect quite different results in these models when the RGE is included. Similarly, $(\mathcal{O}_{Hq}^{(1)})_{33}$ and $(\mathcal{O}_{HQ}^{(3)})_{33}$ occur at tree level in the T VLQ model, and RGE generates $\mathcal{O}_{H\Box}$ at the weak scale which is strongly constrained. On the other hand, the operators generated at tree level in the 2HDM do not contribute to the RG evolution of C_{HD} or $C_{H\Box}$ and we will see that RGE has a relatively minor effect on the interpretation of this model. In our numerical results, we include the complete RGE of all the operators that contribute to our fits.

B. Models

a. Singlet Scalars

One of the simplest extensions to the Standard Model is obtained by adding an additional scalar that is a singlet under the SM gauge group. The scalar potential can be constructed both with and without a Z_2 symmetry. The case without a Z_2 symmetry is particularly interesting because it can accommodate a first order electroweak phase transition for some values of the parameters [32, 33]. Using the classical equations of motion [7, 15, 34, 35], the heavy scalar can be integrated out at tree level, generating the SMEFT operators, $\mathcal{O}_H$ and $\mathcal{O}_{H\Box}$ with coefficients,

$$\begin{aligned} \frac{v^2}{\Lambda^2} C_{H\Box} &= -\frac{1}{2}\tan^2\theta\,, \\ C_H &= -C_{H\Box}\left(\tan\theta\frac{m}{3v} - \kappa\right), \end{aligned} \tag{7}$$

where θ is the mixing angle between the SM-like Higgs boson, h, and the new heavy scalar and κ and m are Lagrangian parameters that are limited by the requirement that the electroweak minimum be the lowest minimum of the potential [36]. In this model, the SM-like Higgs couplings to SM particles are uniformly suppressed by a factor of $\cos\theta$ and for the case with a Z_2 symmetry, there is a cancellation implying $C_H = 0$ [15, 35]. Details of the model are in Appendix A 1.

b. A Second Higgs Doublet

The 2 Higgs doublet model (2HDM) has been extensively studied in the literature, and in the limit that the new Higgs bosons are much heavier than the SM-like Higgs bosons, the Higgs couplings approach those of the SM [37]. This is the alignment limit, $\cos(\beta-\alpha) \to 0$. In the exact alignment limit, SMEFT operators are not generated at tree level, but first appear at 1-loop. Away from the alignment limit, $\cos(\beta-\alpha) \ll 0$, tree level contributions to the Higgs-Yukawa couplings are generated, along with a correction to the Higgs tri-linear coupling. To linear order in $\cos(\beta-\alpha)$, the SMEFT coefficients that affect Higgs couplings to fermions, f, are [6, 15, 38, 39],

$$\frac{v^2 C_{fH}}{\Lambda^2} = -Y_f \eta_f \frac{\cos(\beta-\alpha)}{\tan\beta}\,, \tag{8}$$

where $Y_f = \sqrt{2}m_f/v$ and η_f distinguishes the type of 2HDM and is defined in Appendix A 2. The corrections to the WWh vertex are $\mathcal{O}[\cos^2(\beta-\alpha)]$ and are neglected

in our approximation, since they are formally of dimension-8. The correction to the $\mathcal{O}_H$ operator scales slightly differently,

$$\frac{v^2 C_H}{\Lambda^2} = \frac{\cos^2(\beta-\alpha) M^2}{v^2}\,, \tag{9}$$

where M is the common mass of the heavy decoupled scalars near the alignment limit. We stress that our results are only valid near the alignment limit, where $\cos(\beta-\alpha) \ll 1$and terms of $\mathcal{O}[\cos^2(\beta-\alpha)]$ are systematically neglected. Further details of the model are found in Appendix A 2.

c. Colored Extensions of the SM: an $SU(3)$ Triplet, $SU(2)_L$ Singlet Fermion

We consider a charge $Q = \frac{2}{3}$ color triplet, $SU(2)_L$ singlet fermion, T, and call this the T VLQ (vector-like quark) model and assume that this new quark only couples to the top quark, but not to the lighter quarks. The model is parameterized by 3 parameters: m_t and M_T are the masses of the physical top and new heavy charge $Q = \frac{2}{3}$ fermion respectively, and s_L^t is the sine of a mixing angle that defines the mixing between the left-handed charge $\frac{2}{3}$ quarks. Integrating out the heavy fermion generates the SMEFT coefficients involving the third generation quarks only [6, 40–43]

$$\frac{v^2}{\Lambda^2}\big(C_{Hq}^{(1)}\big)_{33} \;=\; -\frac{v^2}{\Lambda^2}\big(C_{Hq}^{(3)}\big)_{33} = \left(\frac{1}{2Y_t}\right)\frac{v^2}{\Lambda^2}C_{tH} = \frac{(s_L^t)^2}{2} \tag{10}$$

where

$$\begin{aligned}
\big(\mathcal{O}_{Hq}^{(1)}\big)_{33} &= (H^\dagger i \overleftrightarrow{D}_\mu H)(\bar{q}_L^3 \gamma^\mu q_L^3) \\
\big(\mathcal{O}_{Hq}^{(3)}\big)_{33} &= (H^\dagger i \overleftrightarrow{D}_\mu^a H)(\bar{q}_L^3 \tau^a \gamma^\mu q_L^3) \\
\mathcal{O}_{tH} &= (H^\dagger H)(\bar{q}_L^3 \tilde{H} t_R)\,,
\end{aligned} \tag{11}$$

$\bar{q}_L^3 = (\bar{t}_L, \bar{b}_L)$, and the scale Λ is identified with M_T. The corresponding coefficients for the first 2 generations are zero in this model.

Although we perform the matching at tree level, we also include $\mathcal{O}_{HG}$ since it could potentially make a significant contribution to Higgs production through gluon fusion,

$$\frac{v^2}{\Lambda^2}C_{HG} = \frac{\alpha_s}{8\pi}(s_L^t)^2\left(F_{1/2}(M_T) - F_{1/2}(m_t)\right) \sim \mathcal{O}\left(\frac{\alpha_s (s_L^t)^2 m_t^2}{M_T^2}\right), \tag{12}$$

where $F_{1/2}$ is defined in Appendix A 3 a. For $M_T = 1\,\text{TeV}$ ($2\,\text{TeV}$), $F_{1/2}(M_T) - F_{1/2}(m_t) \sim -.010$ ($-.011$) and the top and T contributions approximately cancel in the large m_t

limit. A summary of the model is in Appendix A 3 a.

d. Colored Extensions of the SM: an $SU(3)$ Triplet, $SU(2)_L$ Doublet Fermion

We next consider a model with an $SU(2)_L$ doublet, color triplet pair of vector-like fermions. We term this the (TB) VLQ model. At tree level, the (TB) doublet generates O_{Ht}, O_{Hb}, O_{Htb}, O_{tH}, and O_{bH}, where the operators are defined in Table I in terms of 3^{rd} generation fermions. In the decoupling limit, $M_T, M_B \gg M_Z$,

$$\begin{aligned}
\frac{v^2}{\Lambda^2}C_{Ht} &= -\frac{v^2}{\Lambda^2}\frac{C_{tH}}{Y_t} = -(s_R^t)^2 \\
\frac{v^2}{\Lambda^2}C_{Hb} &= \frac{v^2}{\Lambda^2}\frac{C_{bH}}{Y_b} = (s_R^b)^2 \\
\frac{v^2}{\Lambda^2}C_{Htb} &= 2s_R^t s_R^b,
\end{aligned} \tag{13}$$

where s_R^t and s_R^b define the mixing between the top and bottom quarks with T and B respectively in the right-handed sector. At one-loop, $\mathcal{O}_{HG}$ is also generated,

$$\begin{aligned}
\frac{v^2}{\Lambda^2}C_{HG} &= \frac{\alpha_s}{8\pi}\left((s_R^t)^2\left[F_{1/2}(M_T) - F_{1/2}(m_t)\right] + (s_R^b)^2 F_{1/2}(M_B)\right) \\
&\sim \frac{\alpha_s}{8\pi}(s_R^b)^2(.32)\,,
\end{aligned} \tag{14}$$

where $M_T = M_B = 1\,\text{TeV}$ in the last equation. The approximate cancellation between the t and T contributions found in the T VLQ model remains, but there is an additional contribution from M_B. Details can be found in Appendix A 3 b.

e. Colored Extensions of the SM: an $SU(3)$ Triplet Scalar

Finally, we consider a model with a color triplet complex scalar, s, with charge $Q = \frac{2}{3}$ and mass, m_s. At tree level, four fermion operators that do not contribute to our global fit are generated, but no dimension-6 EFT operators arise. At one loop, the colored scalar generates $\mathcal{O}_{HG}$,

$$\frac{v^2 C_{HG}}{\Lambda^2} = -\frac{\alpha_s \kappa v^2}{96\pi m_s^2}\,, \tag{15}$$

where κ is the portal coupling, $(s\,s^*)\left(H^\dagger H\right)$, and is defined in Appendix A 3 c. This is an example of a model where the only effect on single Higgs production is to rescale the rate and the SMEFT formalism is not necessary. The indirect consequences of the colored scalar and the corresponding SMEFT effects can be searched for in Higgs plus jet or double Higgs production [44, 45].

C. Summary of Models

In Table II, we summarize the coefficients generated by our benchmark models as described in the previous sections, expressing the results in terms of the physical parameters of these models when possible. The scale Λ is consistently identified with the mass of the heavy particle in the model. More precise definitions of these parameters are given in the Appendices.

	Singlet$_{\not\mathbb{Z}_2}$	Singlet$_{\mathbb{Z}_2}$	2HDM	T VLQ	(TB) VLQ	s
$\frac{v^2 C_H}{\Lambda^2}$	$\frac{\tan^2\theta}{2}(\tan\theta\frac{m}{3v}-\kappa)$		$\frac{\cos^2(\beta-\alpha)M^2}{v^2}$			
$\frac{v^2 C_{H\Box}}{\Lambda^2}$	$-\frac{\tan^2\theta}{2}$	$-\frac{\tan^2\theta}{2}$				
$\frac{v^2 C_{bH}}{\Lambda^2}$			$-Y_b\eta_b\frac{\cos(\beta-\alpha)}{\tan\beta}$		$Y_b(s_R^b)^2$	
$\frac{v^2 C_{tH}}{\Lambda^2}$			- $Y_t\eta_t\frac{\cos(\beta-\alpha)}{\tan\beta}$	$Y_t(s_L^t)^2$	$Y_t(s_R^t)^2$	
$\frac{v^2 C_{\tau H}}{\Lambda^2}$			$-Y_\tau\eta_\tau\frac{\cos(\beta-\alpha)}{\tan\beta}$			
$\frac{v^2 (C_{Hq}^{(1)})_{33}}{\Lambda^2}$				$\frac{(s_L^t)^2}{2}$		
$\frac{v^2 (C_{Hq}^{(3)})_{33}}{\Lambda^2}$				$-\frac{(s_L^t)^2}{2}$		
$\frac{v^2 C_{Hb}}{\Lambda^2}$					$(s_R^b)^2$	
$\frac{v^2 C_{Ht}}{\Lambda^2}$					$-(s_R^t)^2$	
$\frac{v^2 C_{Htb}}{\Lambda^2}$					$2s_R^t s_R^b$	
$\frac{v^2 C_{HG}}{\Lambda^2}$				$-\frac{\alpha_s(s_L^t)^2}{8\pi}(.02)$	$\frac{\alpha_s(s_R^b)^2}{8\pi}(.65)$	$-\frac{\alpha_s\kappa v^2}{96\pi m_s^2}$

TABLE II: Tree level SMEFT coefficients. We also list C_{HG} which is generated at 1-loop in some models and give numerical values for C_{HG} for heavy masses of 1 TeV. In all cases, we assume the decoupling limit of the models and the parameters are defined in the appendices. Empty spaces correspond to operators not generated at tree level.

III. RESULTS

A. Methodology

We perform a series of fits to Higgs, diboson, and EWPO data with prior assumptions about the relationships between SMEFT coefficients that are motivated by our example models. We take as non-zero only those coefficients generated in a particular model and examine how that choice changes the fits and the interpretations of the fit results. The underlying goal is to see how the fits can potentially constrain the high scale models. All of our fits are performed to linear order in the SMEFT coefficients.

The EWPO fits use the data given in Table III of [14]. This table uses the most accurate SM theoretical predictions available, typically at NNLO accuracy, along with the tree level SMEFT contributions. The LEP-2 data from $e^+e^- \to W^+W^-$ as parameterized in Ref. [3] is included in the global fits. Using the results in the appendix of Ref. [14], it is straightforward to generalize the leading order SMEFT contributions to the χ^2 given there to allow for the quark operators to have different (but diagonal) couplings to the generations. In particular the coefficients involving the b quark can be different from those of the lighter fermions, which is relevant for the T and (TB) VLQ models. We assume that the lepton generations all couple identically. The contribution of the operator $\mathcal{O}_H$ occurs at 2-loops in the SM and is included using the results from Ref. [23].

The diboson (WW and WZ) and Higgstrahlung (WH and ZH) fits use the data from Table IV of [13] and we include NLO QCD. As shown in [13], the diboson and Higgstrahlung fits are extremely sensitive to whether the fit is performed at linear or quadratic order, with the WZ contribution being particularly sensitive to the inclusion of NLO QCD effects. The diboson and VH data contribute to the fits predominantly through the high p_T regime, and so it is important to understand whether the EFT is valid in the regime where it is being applied. An extensive study was performed in Ref. [13], where it was shown that a large portion of the allowed region in the fits corresponds to a strongly coupled theory where higher dimension operators need to be included in future studies (see in particular, Fig. 7 of that paper). This is not true in the fits to EWPO, where the fits fall within the weakly coupled regime. We further consider this question of EFT validity in Ref. [46] for the case of WZ production. In that study, we remove the high

m_T^{WZ} bins and show the effects on the fit. Removing the bin with $m_T^{WZ} > 600$ GeV from the fit, all points satisfy $m_T^{WZ} < \Lambda = 1\,\text{TeV}$ and the EFT is a valid expansion. In this case, the fits to the coefficients affecting the WWZ vertex are degraded by roughly 30%.

Finally, the Higgs predictions use the $80\,\text{fb}^{-1}$ 13 TeV LHC data from ATLAS [47] and the $36 - 137\,\text{fb}^{-1}$ 13 TeV LHC data from CMS [48], along with the 8 TeV data given in Tables 2 and 3 of [3]. The contribution to Higgs production and decay from $\mathcal{O}_H$ occurs at loop order and is included following the prescription of Ref. [25]. The identification of the observables with the SMEFT predictions is made using tree- level calculations (except for C_{HG} and C_H) and compared with the results of Refs. [3, 49] and reasonable agreement is found.

In the following subsections, we present results for our test models and discuss the use of the global EFT fits for extracting information about the underlying models.

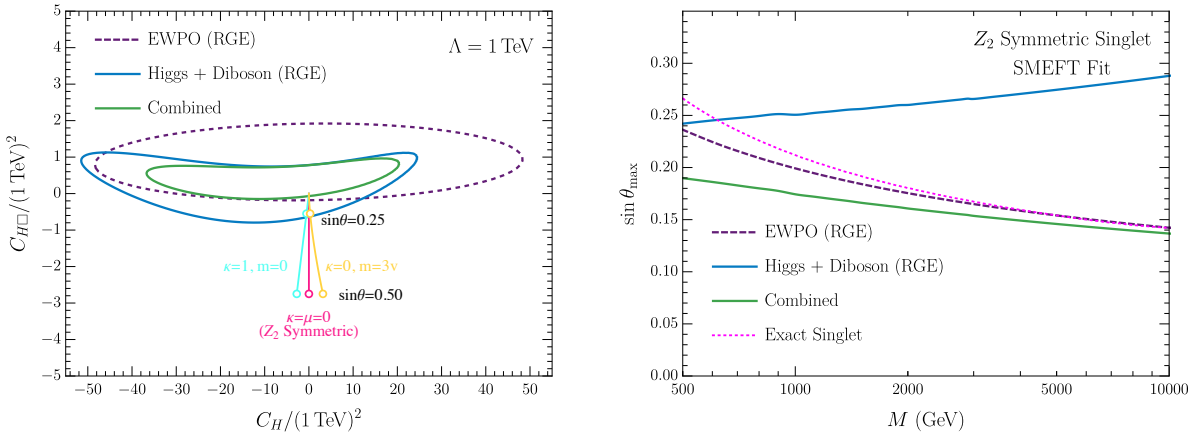


FIG. 1: LHS: 95% C.L. limits on the Wilson coefficients $C_{H\Box}$ and C_H generated at the matching scale. The magenta, cyan, and yellow curves show combinations generated by the singlet model assuming a Z_2 symmetry, and with $\kappa = 1, m = 0$, and $\kappa = 0, m = 3v$, respectively. The open circles indicate the point along the curve with $\sin\theta = 0.25, 0.50$. RHS: The SMEFT coefficient limits reinterpreted in terms of a limit on the mixing angle for the Z_2 symmetric case as a function of the matching scale, M. In both figures, the complete RGE of $C_{H\Box}$ and C_H from $\Lambda = 1\,\text{TeV}$ to the weak scale is included.

B. Model Dependent Results

1. *Singlet Model*

The singlet model generates the two operators, $\mathcal{O}_{H\Box}$ and $\mathcal{O}_H$, at the matching scale Λ, which we take to be M, the mass of the heavier Higgs. We first consider the results of a fit to arbitrary values of the coefficients corresponding to these operators, assuming only that they are generated at the same scale, and taking all other operators to vanish. The results of this fit are shown on the LHS of Fig. 1, where the axes show the coefficients evaluated at the matching scale, $\Lambda = 1\,\text{TeV}$. $\mathcal{O}_{H\Box}$ leads to a shift in the Higgs-gauge couplings, and a universal change in the Higgs couplings to fermions, and these shifts are constrained by LHC data. In addition, via Eq. 6, a non-zero $\mathcal{O}_{H\Box}$ at the matching scale generates the operators $\mathcal{O}_{HD}$, $\mathcal{O}_{Hq}^{(1)}$, and $\mathcal{O}_{Hq}^{(3)}$ at the weak scale, yielding shifts to the EWPOs proportional to $\log(\Lambda/M_Z)$. Numerically, the most important of these operators is $\mathcal{O}_{HD}$,

which generates the T oblique parameter [2]. The limits from EWPOs are shown in Fig. 1 LHS as a purple dashed contour. As anticipated, the limit on C_H is very weak [23, 24]. The constraint from the combination of LHC Higgs and diboson data is shown as a solid blue line, and we see that measurements of the Higgs couplings provide a bound on $C_{H\Box}$ of the same order as the EWPO fit. The combination of LHC data and EWPOs is shown as the solid green curve. In single Higgs data, the operators $\mathcal{O}_{H\Box}$ and $\mathcal{O}_H$ do not generate any momentum dependence, but $\mathcal{O}_{H\Box}$ produces momentum-dependent effects in di-Higgs data which could potentially be of use for the discrimination between models [5, 38, 51].

While we consider first general values of C_H and $C_{H\Box}$, the singlet model generates only a subset of these coefficients. In the Z_2 symmetric case, $C_H = 0$, and $C_{H\Box}$ is always less than zero (see Appendix A 1), so this class of models generates a vertical ray emanating from the origin, shown as a magenta curve in Fig. 1 LHS, with the open circles indicating values of the mixing angle, $\sin\theta = 0.25, 0.50$. The global fit clearly excludes values of $\sin\theta$ above ~ 0.25. Furthermore, in order for the SMEFT to be valid, the coefficients cannot be too large. If we require $\frac{v^2}{\Lambda^2} C_{H\Box} \lesssim \frac{1}{2}$, this would correspond to the requirement that $\sin\theta \lesssim 0.7$, implying that our global fit limits are well within the range of validity of the global fit. Limits on the mixing angle from unitarity and perturbativity of the couplings are considerably weaker than those from the global fits [52].

In the absence of the Z_2 symmetry, the additional couplings lead to more general combinations of C_H and $C_{H\Box}$ at the matching scale, and we show two such combinations, varying the mixing angle, as yellow and cyan rays in Fig. 1 LHS. The values chosen saturate the vacuum stability bounds, Eq. A5, for κ and $m = 0$, respectively. We see that only a small slice of the 2 dimensional SMEFT parameter space at the matching scale can be consistently generated in the singlet model, and that this slice covers only a small part of the allowed range.

With the other coefficients held fixed, the SMEFT limits can be translated into limits on the physical parameter, $\sin\theta$ (defined in Appendix A 1). In the Z_2 symmetric case, it is

[2] The S parameter depends on C_{HWB} which is not generated from RGE in the singlet model. As demonstrated in Ref. [50], in the Warsaw basis there are additional contributions from 4−fermion operators at dimension-6 that are needed to obtain a basis independent result for S. It is also interesting to note from Ref. [6], that only a very small class of models generate $\mathcal{O}_{HWB}$ from dimension-6 operators and none of the models considered here fall into this class.

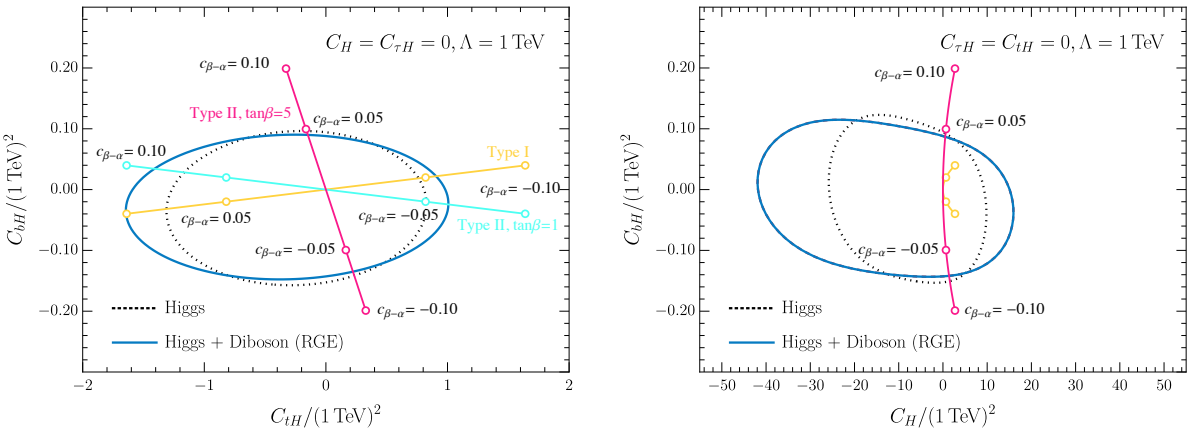


FIG. 2: 95% confidence level limits in the 2HDM from LHC data. All other coefficients are set to zero. The yellow curve corresponds to a Type I model with $\tan\beta = 1$, while the cyan and magenta curves correspond to Type II models with $\tan\beta = 1, 5$ respectively. Open circles along the curve indicate points with $\cos(\beta - \alpha) = \pm 0.05, 0.10$. The coefficients on the axes are evaluated at the matching scale Λ and the curves labelled "Higgs" do not include the RGE of the operators.

apparent from the LHS that $\sin\theta \lesssim 0.25$ for $\Lambda = 1\,\text{TeV}$. More generally, we can interpret limits on the coefficients as limits on the largest allowed mixing angle as a function of the scale, Λ. For the Z_2 symmetric case, $v^2 C_{H\Box}/\Lambda^2 = -\frac{1}{2}\tan^2\theta$, so the only scale dependence is the weak logarithmic dependence from RG evolution, and this is shown on the RHS of Fig. 1. The EWPO limits obtained by fitting the SMEFT coefficients are quite similar to those extracted directly from the EWPOs in the full singlet model [53, 54] as shown by the magenta curve on the RHS of Fig. 1, although there is a roughly 20% difference that can be attributed to the non-logarithmic terms in the complete model calculation [55]. While C_{HD} also appears in the LHC Higgs and diboson data, the bounds on $C_{H\Box}$ arise at tree level, and there are thus different effects in the scaling on the RHS of Fig. 1.

2. 2HDM

The decoupling limit of the 2HDM has been extensively discussed in the literature [37, 56], but here we revisit the question of what information is in the SMEFT fits in the limit where the new scalars are too heavy to be observed. In Appendix A 2, we see that the 2HDM generates $\mathcal{O}_H$, $\mathcal{O}_{uH}$, $\mathcal{O}_{dH}$ and $\mathcal{O}_{eH}$ at tree-level, assuming a small deviation from

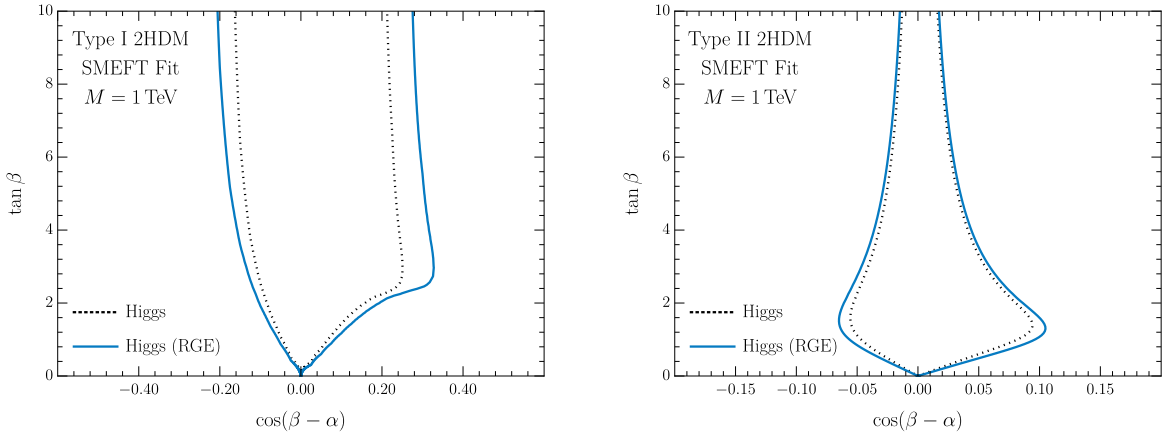


FIG. 3: 95% C.L. limits using the SMEFT fit on the Type I and Type II 2HDM from LHC data in the $\cos(\beta-\alpha)$ vs. $\tan\beta$ plane. The curves labelled "Higgs" do not include the RGE of the operators. Note that our results are formally only valid in the $|\cos(\beta-\alpha)| \ll 1$ limit.

the alignment limit, $|\cos(\beta-\alpha)| \ll 1$. In general, these operators can have arbitrary coefficients for each generation, but to avoid flavor-changing neutral currents, they are usually assumed to be proportional to the SM Yukawa matrices, so — in the limit that only the third generation Yukawas are non-zero — we can consider only the 33 components of these fermionic operators, and label them $\mathcal{O}_{tH}$, $\mathcal{O}_{bH}$, and $\mathcal{O}_{\tau H}$ [3].

None of these operators contribute to the EWPOs at tree level, nor do they generate any of the operators in Eq. 6 at leading logarithm, so we consider only LHC constraints. In Fig. 2, we consider the limits in the C_{tH}–C_{bH} plane (LHS) and the C_H–C_{bH} plane (RHS), in each case setting all other operators to zero. The dashed line shows a fit to Higgs data with the scale-dependence of the operators neglected, while the solid blue curves show the results of a fit where the operators are generated at $\Lambda = 1\,\text{TeV}$ and then RG evolved down to M_Z. On the LHS, we see that the RGE has a minor effect, running the Yukawa-like operators to smaller values in the UV, and resulting in slightly weaker bounds on the coefficients. As in the singlet model case, we see that C_H is only very weakly constrained, and note that the effect of the RGE on the RHS is significant in this case.

In both panels of Fig. 2, we show the patterns of coefficients generated by different

[3] Consistent models with large Yukawa couplings to the first and second generations can also be constructed [57–59].

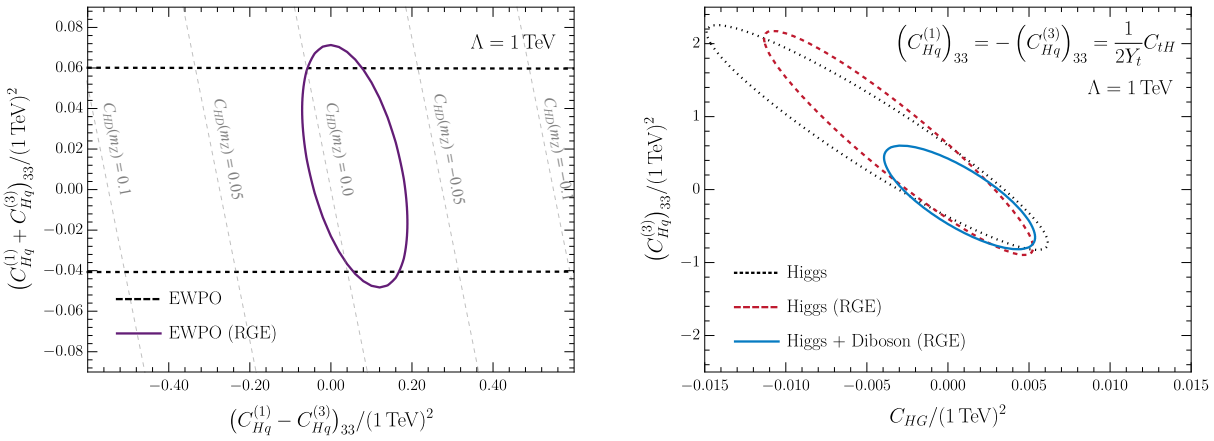


FIG. 4: LHS: 95% confidence level limits from EWPOs (LHS) and RHS: Limits from Higgs and diboson data with SMEFT coefficients in the pattern generated in the T VLQ model. The curve labelled "Higgs" does not include RGE effects. The coefficients on the axes are evaluated at $\Lambda = 1\,\mathrm{TeV}$.

choices of the Glashow-Weinberg conditions [60] for the proportionality constants in the fermion-Higgs operators. The yellow curve corresponds to a Type I model with $\tan\beta = 1$, while the cyan and magenta curves correspond to Type II models with $\tan\beta = 1, 5$ respectively. Note that the $\tan\beta = 1$ curves for the Type I and Type II models are indistinguishable on the RHS. The distances along these curves correspond to different values of the alignment parameter, and we indicate values of $\cos(\beta-\alpha) = \pm 0.05$ and ± 0.1 by open circles. We see that most of the allowed parameter space in the C_{tH} vs. C_{bH} plane can be generated by considering different classes of 2HDMs with different values of $\cos(\beta-\alpha)$ and $\tan\beta$.

The fit to SMEFT coefficients is re-interpreted in terms of the parameters of the 2HDM in Fig. 3, for both the Type I and Type II models near the alignment limit with $M = 1\,\mathrm{TeV}$. These fits show good agreement with the fits in the full, UV complete 2HDM [39]. In the Type I 2HDM, the effects of the RGE reduce the value of C_{tH} when scaling from M_Z to Λ as observed in Fig. 2 and are manifest in the difference between the solid and dashed line in Fig. 3 as well.

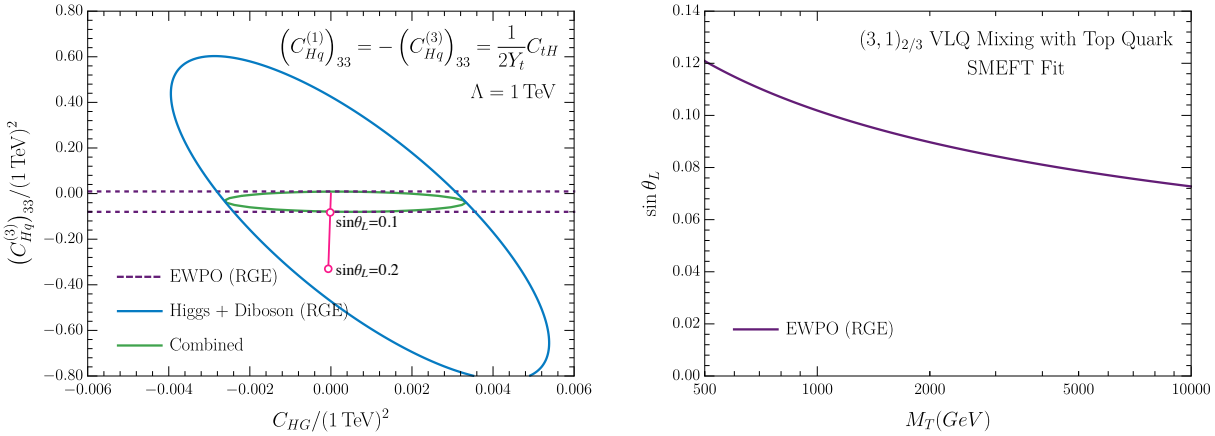


FIG. 5: LHS: Global fit limits with coefficients in the pattern generated in the T VLQ. The green line is the combination of EWPOs, Higgs, and diboson data, with all RGE effects included. The magenta line demonstrates the dependence on the mixing angle corresponding to the SMEFT fits with $s_L^t \equiv \sin\theta_L$. The coefficients on the axes are evaluated at $\Lambda = 1\,\text{TeV}$. RHS: A translation of the limits of the LHS to the parameters of the T VLQ model.

3. Heavy Colored particles in Loops: T VLQ

The case of a heavy $Q = \frac{2}{3}$ vector-like quark coupling only to the third generation leads to the operators $\mathcal{O}_{tH}$, $\left(\mathcal{O}_{Hq}^{(1)}\right)_{33}$ and $\left(\mathcal{O}_{Hq}^{(3)}\right)_{33}$ at tree-level, as well as $\mathcal{O}_{HG}$ at one loop. Importantly, we note that only the third generation operators appear, so fits treating these fermion operators universally are impossible to interpret in the context of these models.

We first consider the constraints on only $\left(C_{Hq}^{(1)}\right)_{33}$ and $\left(C_{Hq}^{(3)}\right)_{33}$ from EWPOs. The dominant effect at tree-level is in the $Z \to b\bar{b}$ decay, which depends only on the combination $\left(C_{Hq}^{(1)} + C_{Hq}^{(3)}\right)_{33}$. This is indicated by the horizontal dashed black lines in Fig. 4 LHS. At leading logarithm, this degeneracy is broken and both $\left(C_{Hq}^{(1)}\right)_{33}$ and $\left(C_{Hq}^{(3)}\right)_{33}$ contribute to the anomalous dimension of $\mathcal{O}_{HD}$. Lines of constant $C_{HD}(M_Z)$ generated from the RGE are shown as dashed gray lines in Fig. 4 LHS, and the resulting limit from the EWPOs including the RGEs, shown as a solid purple curve, clearly follows this shape. It is clear that to draw any conclusions about this model from the EWPOs including both the RGE effects and the non-universality of the fermion operators is crucial.

On the RHS, we consider the limits from Higgs and diboson data. As is apparent from Table II, in the context of the T VLQ, the Wilson coefficients that are generated all come

with a fixed pattern, since there is only one independent physical parameter. To illustrate the importance of this, we thus fix all the relationships between the coefficients except for C_{HG} and plot in the $\left(C_{Hq}^{(3)}\right)_{33} = -\left(C_{Hq}^{(1)}\right)_{33} = -C_{tH}/Y_t$ vs. C_{HG} plane. The resulting limits are highly correlated, and we see that including the effects of the RGE on the fit with only Higgs data (going from dotted black to dashed red lines) has a mild effect on the fits. Most of the limit in the vertical direction, however, comes from including the diboson data, and this dependence arises because the RGE generates $\mathcal{O}_{H\Box}$, which is well constrained by VH and VV fits [13, 61].

Fig. 5 LHS uses the same set of correlations for the Wilson coefficients, and compares the EWPOs constraint (purple, dashed) with the Higgs plus diboson constraint (blue, solid), all with the RGE included. The EWPOs still set a superior limit on the fermionic operators from the RGE induced $\mathcal{O}_{HD}$, while the Higgs data sets the bound on $\mathcal{O}_{HG}$. The combined limit is shown in solid green. In magenta, we show the full prediction of the model, with $\mathcal{O}_{HG}$ related to the other operators via Eq. 12 and open circles indicating a mixing angle of $\sin\theta_L \equiv s_L^t = 0.1, 0.2$. As noted above, the T VLQ generates only a 1-dimensional slice of the parameter space, and while a small value of C_{HG} can be generated, the values corresponding to the model are still nearly orthogonal to the EWPO constraints so that the LHC data is less important in setting a bound on the physical parameter. It is clear that for $M_T = 1\,\text{TeV}$, s_L^t is restricted to < 0.1. The RHS of Fig 5 interprets the SMEFT results as limits on this mixing angle as a function of the T VLQ mass. As in our other examples, the dependence on the scale is only logarithmic, from the RG evolution.

It is of interest to consider how well the global fit limits using the SMEFT coefficients reproduce the constraints found in the complete T VLQ model. A simple estimate can can found from considering the oblique parameter ΔT. The T VLQ result is given in Eq. A18, while the SMEFT limit is derived in Eq. A17 of Appendix A 3. The SMEFT construction reproduces the $\log(\frac{M_T}{m_t})$ terms, but not the constant terms, in ΔT. The ratio of the ΔT parameter in the SMEFT limit to the full result is shown in Fig. 6. Even for quite small values of the mixing parameter, there is a roughly ~ 20 % difference between the results obtained in the SMEFT with tree level matching and one-loop RG running, as compared to the full theory for a fixed value of $\sin\theta_L^t$. However, in order for the T VLQ model to remain weakly coupled, the parameters of the Lagrangian need to scale as $\sin\theta_L^t \sim \frac{1}{M_T}$ [41]. This limit is also shown in the figure, and again the SMEFT limits

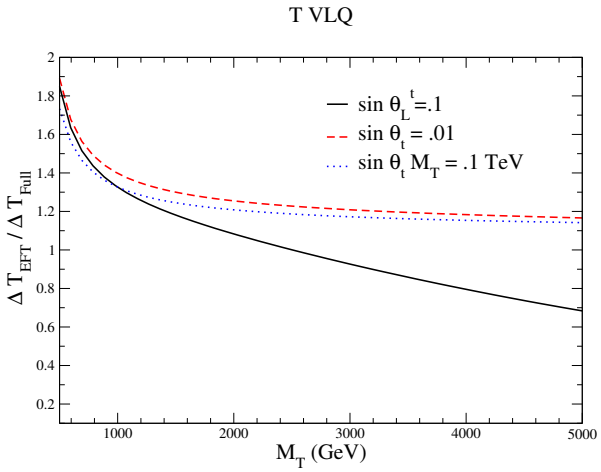


FIG. 6: The ratio of the oblique parameter ΔT in the SMEFT limit with RGE to the result in the full T VLQ model for various values of the mixing parameter.

differ by ~ 20 % from those of the full theory.

4. Heavy Colored particles in Loops: $(T\,B)$ VLQ

In the $(T\,B)$ VLQ model, the operators $\mathcal{O}_{Ht}$, $\mathcal{O}_{Hb}$, $\mathcal{O}_{tH}$, $\mathcal{O}_{bH}$ and $\mathcal{O}_{Htb}$ are generated at tree level, and we emphasize again that only the third generation fermion operators appear. As in the T VLQ model, the only tree-level contribution to EWPOs is through the $Z \to b\bar{b}$ decay, which now directly constrains C_{Hb}. This is shown as the dashed black lines on the LHS of Fig. 7, where we show the SMEFT limits in the C_{Hb} vs. C_{Ht} plane, with the coefficients of all other operators fixed to zero. At tree level, the EWPOs are independent of C_{Ht}, but both C_{Hb} and C_{Ht} generate C_{HD} via the RGE at leading logarithm. The contours of constant C_{HD} (with the slope fixed by the relative values of Y_t and Y_b, as expected from Eq. 6) are shown in dashed gray, and we again see that the EWPO limit including the RGEs (purple, solid) follows this pattern.

The limits coming from Higgs data and diboson data are illustrated on the RHS of Fig. 7. Here, we include the operators $\mathcal{O}_{tH}$, $\mathcal{O}_{Ht}$ and $\mathcal{O}_{HG}$ at the matching scale, with the coefficients of other operators taken to be zero, and then project onto the plane where $C_{tH} = -Y_t\, C_{Ht}$, as predicted by the $(T\,B)$ VLQ. Similarly to the T VLQ case, the importance of the diboson data is apparent when the RGE of the coefficients from the matching scale to the weak scale is included, as a nonzero C_{Ht} at the matching scale leads to values of C_{HD} at the weak scale that are well constrained by diboson data. A

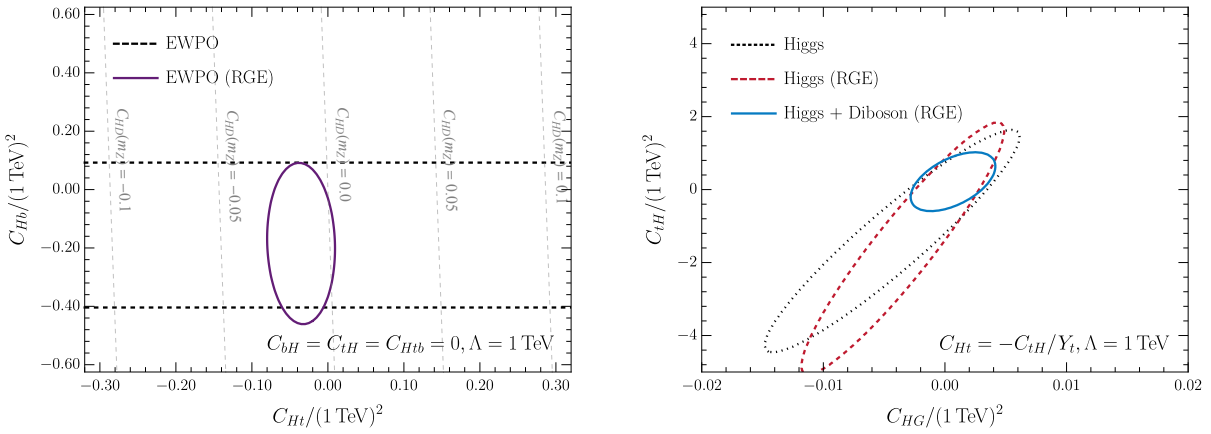


FIG. 7: LHS: 95% confidence level limits on C_{Ht} and C_{Hb} when all other coefficients are set to zero from EWPOs. RHS: Same, but including the RG evolution from the matching to the weak scale. The coefficients on the axes are evaluated at $\Lambda = 1\,\text{TeV}$.

similar story pervades three of our example models: if a C_{HD} or $C_{H\Box}$ appear at leading logarithm in the anomalous dimensions for the operators generated at the matching scale, the diboson data can place important constraints that may not be apparent in the tree-level matching.

In Fig. 8 LHS, we directly compare the EWPO and Higgs plus diboson constraints by considering the SMEFT fits in the C_{Ht} vs. C_{Hb} plane. To include the effects of all the operators, we again set $C_{tH} = -Y_t\, C_{Ht}$, and similarly set $C_{bH} = -Y_b\, C_{Hb}$. We also include $\mathcal{O}_{HG}$ with $C_{HG} = 0.65\left(\alpha_s/8\pi\right) C_{Hb}$, as implied by Eq. 14 for $M_T = M_B = 1\,\text{TeV}$. We see that, even including all of these correlations, the EWPO constraint still sets a superior bound to the Higgs plus diboson data.

In contrast with the T VLQ, the $SU(2)_L$ doublet VLQ model has two independent parameters in the decoupling limit, the two mixing angles $\sin\theta_R^b \equiv s_R^b$ and $\sin\theta_R^t \equiv s_R^t$, or equivalently, s_R^b and the mass splitting, $\delta M_{TB} = M_T - M_B$ (see Appendix A 3 b for details). In the limit $\delta M_{TB} = 0$, the mixing angles are identical, and $C_{Hb} = C_{Ht}$. This is indicated by the magenta line in Fig. 8 LHS. Allowing for a nonzero mass splitting, however, shifts this relation, as can be seen by the yellow line in Fig. 8 LHS for $\delta M_{TB} = 10\,\text{GeV}$. It is obvious from this shift that the EWPOs set a strong constraint on the mass splitting for fixed s_R^b via the RGE induced C_{HD}. This is simply a manifestation of the strong constraint on custodial symmetry violation, which we comment more on in Appendix A 3 b. The

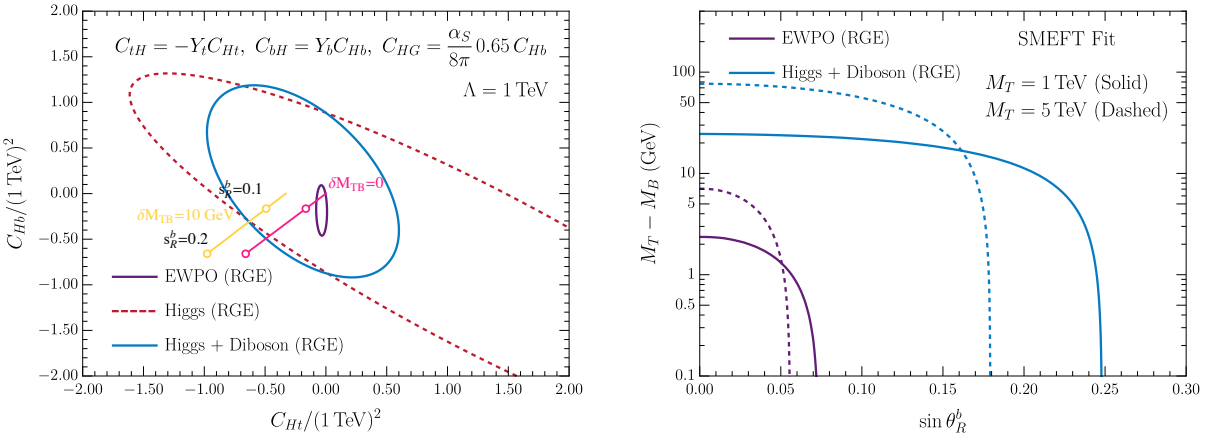


FIG. 8: LHS: 95% confidence level limits on C_{Ht} and C_{Hb} when the other coefficients are set to the correlated values of the $(T\,B)$ VLQ model with $M_T = M_B$ at the matching scale and including RG evolution of the coefficients to M_Z. The magenta and yellow lines correspond to predictions for the coefficients with $\delta M_{TB} = 0$ and $\delta M_{TB} = 10$ GeV. The coefficients on the axes are evaluated at $\Lambda = 1\,\text{TeV}$. RHS: Limits on the mass splitting of the $(T\,B)$ VLQ using the model correlations given in Table II.

behavior in Fig. 8 also illustrates that varying the two mixing angles sweeps out a region in the C_{Ht} vs. C_{Hb} plane, but that there is still a very tight relationship between all five operators generated by the model, which changes the interpretation of the global fits in this context significantly.

On the RHS of Fig. 8, we reinterpret the SMEFT bounds in the δM_{TB} vs. s_R^b plane, showing both the EWPO constraint (purple) and the Higgs plus diboson constraint (blue). We show the results for both $M_T = 1\,\text{TeV}$ (solid) and $M_T = 5\,\text{TeV}$ (dashed), and note that the logarithmic dependences on δM_{TB} and s_R^b have opposite signs.

C. Global Fit to SMEFT Coefficients

As a by-product of our study, we present an updated global fit to the 19 SMEFT coefficients considered here in the Warsaw basis. In comparison to Ref. [3], this fit includes higher integrated luminosity data from ATLAS [47] and CMS [48], as well as the NLO QCD corrections to VV and VH production with the full distributions as in Ref. [13]. The results are shown in Fig. 9 with each coefficient treated individually and in Fig. 10

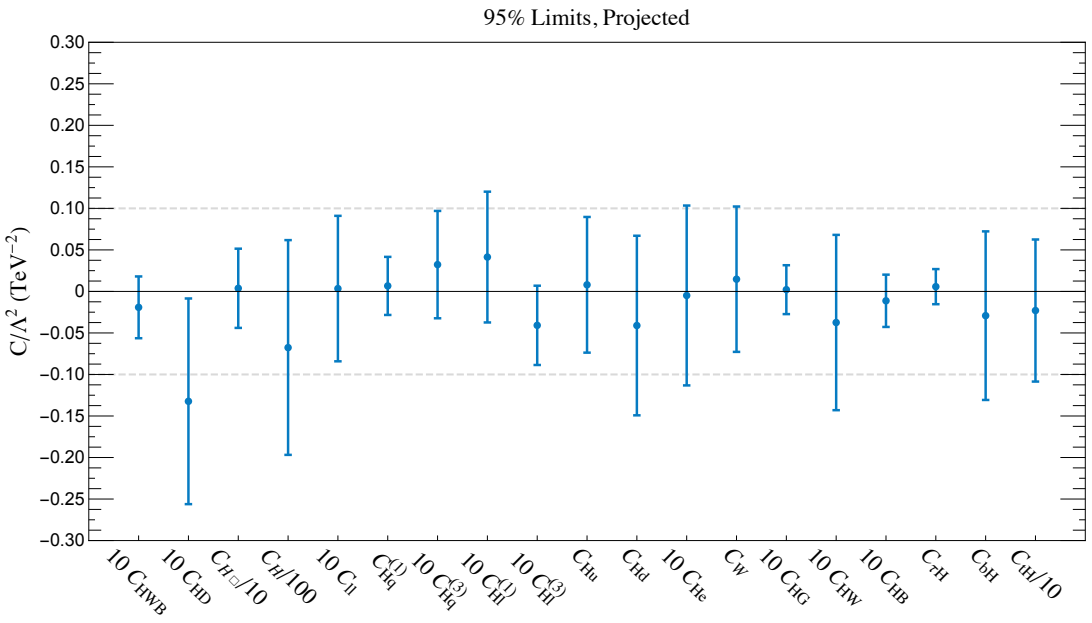


FIG. 9: 95% C.L. limits on the coefficients of operators, with all other coefficients set to zero. The bounds on operators involving fermions assume universal coefficients, except for C_{bH}, C_{tH}, and $C_{\tau H}$, which modify only the third-generation Yukawa couplings.

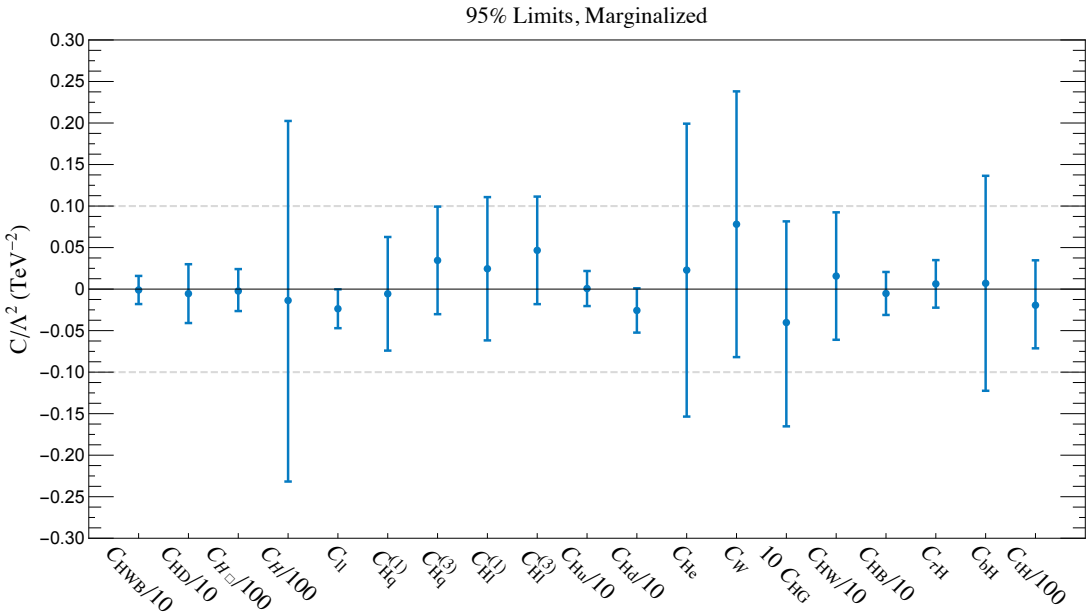


FIG. 10: 95% C.L. limits on each the coefficients of each operator, marginalizing over all other operators. We assume universal coefficients for operators involving fermions, except for C_{bH}, C_{tH}, and $C_{\tau H}$, which modify only the third-generation Yukawa couplings.

when marginalizing over all the couplings. The result for $C_{Hq}^{(3)}$ is considerably strengthened from that of Ref. [3], due to the inclusion of the WZ data not available in that work. . In general, the inclusion of the higher luminosity Higgs data strengthens the limits that are not dominated by EWPO data by $\mathcal{O}(20\%)$. Note that, in contrast to many of our particular model fits, here we assume universal couplings to the quark operators $C_{Hq}^{(1)}$, $C_{Hq}^{(3)}$, C_{Hu} and C_{Hd}. The assumption that the quark couplings are flavor blind has a major effect on the fits, as the constraints now have a significant contribution from diboson and Higgstrahlung production from first-generation quarks. Numerical values for the fits can be found at https://quark.phy.bnl.gov/Digital_Data_Archive/dawson/smeft_20.

IV. DISCUSSION

A major goal of precision measurements at the LHC is to uncover hints of new physics through patterns of deviations from the SM. In this work, we examine how fits to SMEFT coefficients that are predicated on patterns of coefficients generated in different UV complete models give information about the high scale physics. Of particular interest to us are the assumptions made when forming inferences about the source of new physics from SMEFT fits.

Only two of our models, the Z_2 non-symmetric singlet model and the 2HDM generate a shift in the Higgs tri-linear coupling C_H. In the singlet model, this shift is correlated with a non-zero $C_{H\Box}$ term that can be observed in VV and VH production. In the 2HDM, the non-zero C_H is directly proportional to the C_{fH} interaction and a weak limit on C_H is obtained. The 2HDM and the $(T\,B)$ VLQ models generate C_{fH} terms that can be directly measured in Higgs production at the LHC. The $(T\,B)$ model also generates C_{Hf} couplings that are limited by precision Z measurements. When the fits are performed using the patterns of coefficients predicted in each model, the results are quite different from the global fit results and in all cases, the correlated fits deviate significantly from the single parameter fits.

An interesting feature of our work is the importance of the RGE on the interpretation of the fits. This suggests that redoing the study with complete one-loop matching would be of interest. If a model predicts coefficients at the matching scale that generate operators through RGE that are constrained by EWPOs or diboson data, then these coefficients

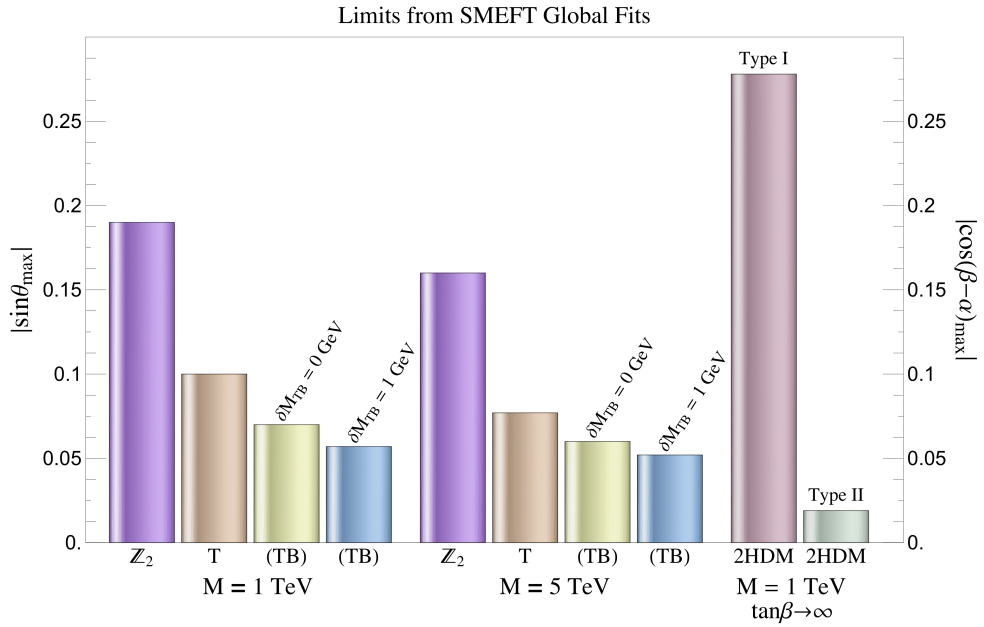


FIG. 11: Maximum allowed mixing angles as a function of the heavy particle mass from the SMEFT global fit. Note that the 2HDM limits are valid in the $|\cos(\beta-\alpha)| \ll 1$ limit.

are strongly constrained. The inclusion of RGE completely changes the interpretation of the fits in these cases.

In Fig. 11, we summarize our SMEFT results in terms of the physical parameters of the models and show the maximum allowed mixing angle from the global fits in each model as a function of scale. We note that these are the limits in the SMEFT where the heavy particles have been integrated out of the UV complete model. The fits are sensitive to the ratios C_i/Λ^2, modulo the logarithmic dependence from the RG running.

Our study is just the beginning of an understanding of the discrimination between UV theories from SMEFT fits [62]. Follow-up work could include information from top physics [63–68], a consideration of the importance of the quadratic versus linear SMEFT approximation [13], and complete 1-loop matching. The complete 1-loop matching contributions exist for the singlet model [16, 69, 70], but not for the VLQ models where there are missing heavy-light contributions [71, 72]. The inclusion of flavor observables (such as B and K data) into the fit could further restrict the allowed coefficients in the various models [73–77]. It is of considerable interest to expand our study by examining further concrete example models and performing detailed comparisons of the SMEFT fits with the global fits in the complete models.

Acknowledgments

SD is supported by the United States Department of Energy under Grant Contract DE-SC0012704. The work of SH was supported in part by the National Science Foundation grant PHY-1915093. SL is supported by the State of Kansas EPSCoR grant program and the U.S. Department of Energy, Office of Science, Office of Workforce Development for Teachers and Scientists, Office of Science Graduate Student Research (SCGSR) program. The SCGSR program is administered by the Oak Ridge Institute for Science and Education (ORISE) for the DOE. ORISE is managed by ORAU under contract number DE-SC0014664. Digital data can be found at https://quark.phy.bnl.gov/Digital_Data_Archive/dawson/smeft_20.

Appendix A: Additional Details on the Models

1. Singlet Scalar

The most general scalar potential involving a real scalar singlet, $\tilde{S}$, and the SM $SU(2)_L$ doublet, H, is ,

$$\begin{aligned} V &= -\mu_h^2 \mid H \mid^2 + \frac{\lambda_h}{2}(\mid H \mid^2)^2 + \frac{m_S^2}{2}\tilde{S}^2 + A \mid H \mid^2 \tilde{S} \\ &+ \frac{\kappa}{2} \mid H \mid^2 \tilde{S}^2 + \frac{m}{6}\tilde{S}^3 + \frac{\lambda_S}{24}\tilde{S}^4. \end{aligned} \tag{A1}$$

The parameters can be redefined such that $\langle \tilde{S} \rangle = 0$. After spontaneous symmetry breaking, the 2 neutral scalars, $H_0 = (\tilde{h} + v)/\sqrt{2}$ and $\tilde{S}$, mix to form the physical scalars, h and S,

$$\begin{aligned} h &= \cos\theta\, \tilde{h} - \sin\theta\, \tilde{S} \\ S &= \sin\theta\, \tilde{h} + \cos\theta\, \tilde{S}\,, \end{aligned} \tag{A2}$$

with the physical masses, m_h and M. We assume $M \gg m_h$. The heavy scalar can be integrated out [7, 15, 34, 35], generating the 2 operators, $\mathcal{O}_H$ and $\mathcal{O}_{H\Box}$ with coefficients,

$$\begin{aligned} \frac{C_{H\Box}}{\Lambda^2} &= -\frac{A^2}{2m_S^4} \\ \frac{C_H}{\Lambda^2} &= \frac{A^2}{2m_S^4}\left(\frac{mA}{3m_S^2} - \kappa\right). \end{aligned} \tag{A3}$$

In terms of the physical parameters of the theory $(m_h, M, \sin\theta)$,

$$\begin{aligned}\frac{C_{H\Box}}{\Lambda^2} &= -\frac{1}{2v^2}\left(\frac{(m_h^2-M^2)\sin(2\theta)}{m_h^2+M^2+(M^2-m_h^2)\cos(2\theta)}\right)^2 \\ &\to -\frac{1}{2v^2}\tan^2\theta\,, \\ C_H &\to = -C_{H\Box}\left(\tan\theta\frac{m}{3v}-\kappa\right)\end{aligned} \tag{A4}$$

where in the last lines, we take the $M \to \infty$ limit. Ref. [38] has pointed out that in some cases, an improved agreement between the exact (singlet model) UV theory and the SMEFT can be obtained by retaining the dependence on m_h in Eq. A4. The Lagrangian parameters μ and κ are limited by the requirement that the minimum of the potential be the electroweak vacuum, (see Fig. 1 of Ref. [36]),

$$\begin{aligned}|\,\frac{m}{v}\,| &< 6 \\ |\,\kappa\,| &< 1\,,\end{aligned} \tag{A5}$$

and so fixing $0 < \theta < \frac{\pi}{2}$, $|\,C_H\,| \lesssim |\,2\tan\theta+1\,|\,C_{H\Box}$. In the case where there is a Z_2 symmetry, the potential of Eq. A1 has $A = \mu = 0$. In this case, there is a cancellation in Eq. A3 implying $C_H = 0$ and the singlet vev can no longer be fixed to 0.

2. A Second Higgs Doublet

For the 2 Higgs doublet model, we work in the Higgs basis, where the doublets have been rotated such that only the SM-like doublet, H_1, gets a VEV, v. In this framework, the components of the H_2 doublet can be taken heavy and we work in the decoupling limit where the 2HDM can be matched to the SMEFT coefficients [15, 38, 39, 78]. The scalar potential is [79],

$$\begin{aligned}V_S &= M_1^2\,|\,H_1\,|^2 + M_2^2\,|\,H_2\,|^2 + (Y_3 H_1^\dagger H_2 + h.c.) \\ &\quad + \frac{1}{2}(Z_1\,|\,H_1\,|^4 + Z_2\,|\,H_2\,|^4) + Z_3\,|\,H_1\,|^2|\,H_2\,|^2 + Z_4(H_1^\dagger H_2)(H_2^\dagger H_1) \\ &\quad - \left(\frac{Z_5}{2}(H_1^\dagger H_2)(H_1^\dagger H_2) + Z_6\,|\,H_1\,|^2\,(H_1^\dagger H_2) + Z_7\,|\,H_2\,|^2\,H_1^\dagger H_2 + h.c.\right).\end{aligned} \tag{A6}$$

The Yukawa terms are,

$$\begin{aligned}V_Y &= Y_u \bar{q}_L \tilde{H}_1 u_R + Y_d \bar{q}_L H_1 d_R + Y_e \bar{l}_L H_1 e_R \\ &\quad + \frac{\eta_u Y_u}{\tan\beta}\bar{q}_L \tilde{H}_2 u_R + \frac{\eta_d Y_d}{\tan\beta}\bar{q}_L H_2 d_R + \frac{\eta_e Y_e}{\tan\beta}\bar{l}_L H_2 e_R + \text{h.c.}\,,\end{aligned} \tag{A7}$$

	η_t	η_b	η_τ
Type-I	1	1	1
Type-II	1	$-\tan^2\beta$	$-\tan^2\beta$
Lepton-specific	1	1	$-\tan^2\beta$
Flipped	1	$-\tan^2\beta$	1

TABLE III: 2HDM couplings of fermions.

where $Y_f = \frac{\sqrt{2}m_f}{v}$, $\tilde{H}_i = i\sigma_2 H_i^*$, and the parameters η_f depend on the type of 2HDM and are given in Table III. In general, the Yukawa couplings are 3×3 matrices, but we will always take them diagonal when considering the 2HDM.

We work in the limit $Y_3/M_2^2 \ll 1$ and integrate out the heavy doublet H_2 following Refs. [7, 39]. Since the equations of motion imply $Y_3 = -Z_6 v^2/2$, we also have $|\, Z_6 v^2/M_2^2 \,| \ll 1$. In the decoupling limit, the heavy masses $M_H \sim M_A \sim M_{H^+} \sim M$ and the tree level SMEFT contributions are,[4]

$$\begin{aligned} \frac{C_H}{\Lambda^2} &= \frac{Z_6^2}{M^2} & \frac{C_{uH}}{\Lambda^2} &= \frac{\eta_u Y_u Z_6}{\tan\beta M^2} \\ \frac{C_{dH}}{\Lambda^2} &= \frac{\eta_d Y_d Z_6}{\tan\beta M^2} & \frac{C_{eH}}{\Lambda^2} &= \frac{\eta_e Y_e Z_6}{\tan\beta M^2}\,. \end{aligned} \tag{A8}$$

The 2HDM also generates 4-fermi interactions that do not contribute to our tree- level study. In the decoupling limit,

$$\cos(\beta-\alpha) \approx -\frac{Z_6 v^2}{M^2}\,.$$

Keeping only third generation fermion masses non-zero,

$$\begin{aligned} \frac{v^2 C_H}{\Lambda^2} &= \frac{\cos^2(\beta-\alpha)M^2}{v^2} & \frac{v^2 C_{tH}}{\Lambda^2} &= -\frac{\eta_t Y_t \cos(\beta-\alpha)}{\tan\beta} \\ \frac{v^2 C_{bH}}{\Lambda^2} &= -\frac{\eta_b Y_b \cos(\beta-\alpha)}{\tan\beta} & \frac{v^2 C_{\tau H}}{\Lambda^2} &= -\frac{\eta_\tau Y_\tau \cos(\beta-\alpha)}{\tan\beta}\,. \end{aligned} \tag{A9}$$

Note that we need $\cos(\beta-\alpha)\frac{M^2}{v^2}$ to be small for decoupling [37].

[4] We assume all couplings are real and neglect flavor indices.

3. Colored Extensions of the SM

Finally, we consider extending the Standard Model with new colored fields. In particular, we will consider heavy vector-like quarks, either a singlet or doublet under $SU(2)_L$, and colored triplet scalars.

a. SU(3) Triplet $SU(2)_L$ Singlet Fermion

The T VLQ model has a charge $\frac{2}{3}$ color triplet, $SU(2)_L$ singlet fermion. The particles in the top sector are,

$$\psi_L, T_R^1, T_L^2, T_R^2\,, \tag{A10}$$

where ψ_L, T_R^1 are the SM-like left handed quark doublet and right-handed charge $\frac{2}{3}$ quark and T^2 is the new vector-like quark. The relevant portion of the Lagrangian is,

$$V_Y \;=\; \lambda_2 \overline{\psi}_L \tilde{H} T_R^1 + \lambda_3 \overline{\psi}_L \tilde{H} T_R^2 + \lambda_5 \overline{T}_L^2 T_R^2 + h.c. \tag{A11}$$

which can be expressed in terms of the physical parameters, m_t, M_T, $\sin\theta_L^t \equiv s_L^t$. After the mixing, the physical fermions are,

$$\begin{aligned} t_L \;&=\; \cos\theta_L^t\, T_L^1 - \sin\theta_L^t\, T_L^2 \\ T_L \;&=\; \sin\theta_L^t\, T_L^1 + \cos\theta_L^t\, T_L^2 \end{aligned} \tag{A12}$$

and we define $q_L^3 = (t_L, b_L)^T$ to be the physical third generation fermion doublet. (Note that the mixing in the right-handed quark sector can be rotated away, so there is only one mixing angle in this model.)

In order to obtain decoupling, the Yukawa interactions must be much smaller than the Dirac mass term, $\lambda_2 v,\ \lambda_3 v \ll \lambda_5$. In this limit [41],

$$s_L^t \to \frac{v\lambda_3}{\sqrt{2}M_T}\,, \tag{A13}$$

and

$$\begin{aligned} \lambda_2 \;&\to\; \frac{\sqrt{2}m_t}{v}\left[1 + \frac{(s_L^t)^2}{2}\left(\frac{M_T^2}{m_t^2} - 1\right)\right] \sim Y_t \\ \lambda_3 \;&\to\; \frac{\sqrt{2}M_T}{v} s_L^t \\ \lambda_5 \;&\to\; M_T\left[1 + \frac{(s_L^t)^2}{2}\left(\frac{m_t^2}{M_T^2} - 1\right)\right]. \end{aligned} \tag{A14}$$

Hence, decoupling requires $(s_L^t)^2 \sim \frac{m_t^2}{M_T^2}$ as seen in Eq. A13.

The SMEFT coefficients that are generated at tree level are,

$$\begin{aligned} \frac{v^2}{\Lambda^2}\left(C_{Hq}^{(1)}\right)_{33} &= \frac{\lambda_3^2 v^2}{4M_T^2} = -\frac{v^2}{\Lambda^2}\left(C_{Hq}^{(3)}\right)_{33} \\ \frac{v^2}{\Lambda^2}C_{tH} &= \frac{\lambda_2\lambda_3^2 v^2}{2M_T^2}\,. \end{aligned} \tag{A15}$$

It is clear that there is only 1 independent SMEFT coefficient in this model at tree level.

The T VLQ model generates a contribution to $\mathcal{O}_{HD}$ through the running of $C_{Hq}^{(1)}$,

$$\dot{C}_{HD} = -24\left(C_{Hq}^{(1)}\right)_{33}(Y_b^2 - Y_t^2)\,. \tag{A16}$$

Neglecting the b mass, matching at $\Lambda = M_T$, $\frac{(C_{Hq}^{(1)})_{33}(M_T)}{\Lambda^2} = \frac{(s_L^t)^2}{2}$, and evolving to m_t, we find

$$\begin{aligned} \Delta T_{EFT} &= -\frac{v^2}{2\alpha}C_{HD}(m_t) \\ &= 2(s_L^t)^2 T_{SM}\log\left(\frac{M_T^2}{m_t^2}\right), \quad T_{SM} = \frac{3}{16\pi s_W^2}\frac{m_t^2}{M_W^2}\,, \end{aligned} \tag{A17}$$

reproducing the logarithmic contribution of the UV complete T VLQ model. The complete model, however, has the $s_L^t \to 0$, $M_T \to \infty$ limit [41, 80],

$$\Delta T_{UV} = T_{SM}\left[-2 + (s_L^t)^2\frac{M_T^2}{m_t^2} + 2\log\left(\frac{M_T^2}{m_t^2}\right)\right] \tag{A18}$$

and we note that the SMEFT cannot reproduce the (numerically significant) $(s_L^t)^2 M_T^2/m_t^2$ term of the UV complete model.

The T VLQ generates $\mathcal{O}_{HG}$ at 1-loop,

$$\frac{v^2}{\Lambda^2}C_{HG} = \frac{\alpha_s}{8\pi}(s_L^t)^2\Big(F_{1/2}(M_T) - F_{1/2}(m_t)\Big) \tag{A19}$$

where

$$\begin{aligned} F_{1/2}(\tau) &= \tau\Big[1 + (1-\tau)f(\tau)\Big] \\ f(\tau) &= \left[\sin^{-1}\left(\frac{1}{\sqrt{\tau}}\right)\right]^2 \qquad \tau \gg 1 \end{aligned} \tag{A20}$$

and $\tau = 4m^2/m_h^2$, where $m = m_t, M_T$ and $F_{1/2} \to \frac{2}{3}$ in the $m_t \to \infty$ limit. In the high energy limit, the contribution of C_{HG} to Higgs production is highly suppressed by the cancellation between the top loop and the T loop and there is only a very slight dependence on M_T,

$$\frac{v^2}{\Lambda^2}C_{HG} \sim -\frac{\alpha_s}{8\pi}(s_L^t)^2\frac{7m_h^2}{180m_t^2}\left(1 - \frac{m_t^2}{M_T^2}\right). \tag{A21}$$

b. SU(3) Triplet $SU(2)_L$ Doublet Fermion

We next consider a model with an $SU(2)_L$ doublet and color triplet pair of vector-like fermions. We term this the (TB) VLQ model [6, 41, 81]. The third generation quarks in the (T, B) model are,

$$\psi_L^T = (T_L^1, B_L^1), T_R^1, B_R^1, \chi_L^T \;=\; (T_L^2, B_L^2), \chi_R^T = (T_R^2, B_R^2) \tag{A22}$$

corresponding to the scalar potential,

$$V_S \;=\; \lambda_t \overline{\psi}_L \tilde{H} T_R^1 + \lambda_b \overline{\psi}_L H B_R^1 + \lambda_4 \overline{\chi}_L \tilde{H} T_R^1 + \lambda_5 \overline{\chi}_L H B_R^1 + M \overline{\chi}_L \chi_R + h.c. \tag{A23}$$

(A term $\overline{\psi}_L \chi_R$ can be rotated away by a redefinition of the fields.)

Diagonalizing the mass matrices requires 4 angles in the left- and right- handed $t - T$ and $b - B$ sectors, $\theta_L^t,\ \theta_R^t,\ \theta_L^b, \theta_R^b$. Since there are 5 terms in the Lagrangian, there are 5 independent parameters which we take to be the physical masses and one mixing angle,

$$M_T, m_t, M_B, m_b, s_R^b \,. \tag{A24}$$

For small mixing angles,

$$\begin{aligned} (s_L^t)^2 \;&\sim\; \frac{m_t^2}{M_T^2} (s_R^t)^2 \\ (s_L^b)^2 \;&\sim\; \frac{m_b^2}{M_B^2} (s_R^b)^2 \,. \end{aligned} \tag{A25}$$

The mixing in the right-handed top sector is determined from that in the right-handed bottom sector,

$$(s_R^t)^2 = (s_R^b)^2 \left(\frac{M_B^2 - m_b^2}{M_T^2 - m_t^2} \right) + \left(\frac{M_T^2 - M_B^2}{M_T^2 - m_t^2} \right) . \tag{A26}$$

If the mass splitting between the T, B particles is small, $\delta M_{TB} = M_T - M_B,\ \frac{|\delta M_{TB}|}{M_T} \ll 1$, and $m_t \ll M_T$, the mixing in the top sector is,

$$(s_R^t)^2 = (s_R^b)^2 + (c_R^b)^2 \frac{2 \delta M_{TB}}{M_T} \,. \tag{A27}$$

For small mixing angles, and $m_t \ll M_T$, $m_b \ll M_B$, [82]

$$\begin{aligned} s_R^t \;&=\; \frac{\lambda_4 v}{\sqrt{2} M_T} \\ s_R^b \;&=\; \frac{\lambda_5 v}{\sqrt{2} M_B} \,. \end{aligned} \tag{A28}$$

At tree level, the (TB) doublet model generates $\mathcal{O}_{Ht},\ \mathcal{O}_{Hb},\ \mathcal{O}_{Htb}, \mathcal{O}_{tH},\ \mathcal{O}_{bH}$ [40],

$$\begin{aligned}
\frac{v^2}{\Lambda^2}C_{Ht} &= -\frac{\lambda_4^2 v^2}{2M_T^2} = -(s_R^t)^2 \\
\frac{v^2}{\Lambda^2}C_{Hb} &= \frac{\lambda_5^2 v^2}{2M_B^2} = (s_R^b)^2 \\
\frac{v^2}{\Lambda^2}C_{tH} &= -\frac{\sqrt{2}m_t}{v}\frac{v^2}{\Lambda^2}C_{Ht} \\
\frac{v^2}{\Lambda^2}C_{bH} &= \frac{\sqrt{2}m_b}{v}\frac{v^2}{\Lambda^2}C_{Hb} \\
\frac{v^2}{\Lambda^2}C_{Htb} &= 2s_R^t s_R^b\,.
\end{aligned} \tag{A29}$$

Only C_{Ht} and C_{Hb} are independent and are related by Eq. A27 to the heavy masses. We can consistently take $\Lambda = M_T$ or $\Lambda = M_B$. From the measurement of $Z \to b\bar{b}$, the right-handed coupling to the b is small, $s_R^b < .115$ [83], corresponding to $\frac{v^2}{\Lambda^2}C_{Hb} < .013$, independent of M_B. It is therefore consistent to consider the small s_R^b limit.

Similarly to the T VLQ model, $\mathcal{O}_{HD}$ is generated from the running of $C_{Hu},\ C_{Hd}$ and C_{Hud},

$$\dot{C}_{HD} = -24\left[Y_t^2 C_{Ht} - Y_b^2 C_{Hb} + Y_b Y_t C_{Htb}\right]. \tag{A30}$$

Neglecting the b mass and considering small s_R^b and $\mid \delta M_{TB} \mid /M_T$,

$$\begin{aligned}
\frac{v^2}{\Lambda^2}\dot{C}_{HD} &= 24 Y_t^2 (s_R^t)^2 \\
&\sim 24 Y_t^2\left[(s_R^b)^2\left(1 - \frac{2\delta M_{TB}}{M_T}\right) + \frac{2\delta M_{TB}}{M_T}\right].
\end{aligned} \tag{A31}$$

Even in the $s_R^b \to 0$ limit, the running of $\mathcal{O}_{HD}$ yields a contribution to ΔT proportional to the mass splitting, giving

$$\Delta T_{EFT} \to 8 T_{SM}\frac{\delta M_{TB}}{M_T}\log\left(\frac{M_T^2}{m_t^2}\right), \tag{A32}$$

reproducing the logarithm of the UV complete model [41, 80]. Comparing with Eq. 57 of [41] we see that $\Delta T_{EFT}/\Delta T(\text{full}) \sim 1.4$, implying that the limits obtained in the EFT will be more stringent than the actual limits in the full theory.

At one-loop, $\mathcal{O}_{HG}$ is generated,

$$\begin{aligned}
\frac{v^2}{\Lambda^2}C_{HG} &= \frac{\alpha_s}{8\pi}\left((s_R^t)^2\left[F_{1/2}(M_T) - F_{1/2}(m_t)\right] + (s_R^b)^2 F_{1/2}(M_B)\right) \\
&\sim \frac{\alpha_s}{8\pi}(s_R^b)^2(.65)
\end{aligned} \tag{A33}$$

where $M_T = M_B = 1\,\text{TeV}$ in the last equation. Note that the cancellation between the SM top quark and the T VLQ contribution that was observed in the T VLQ model is weakened due to the presence of two heavy VLQs.

c. SU(3) Triplet Scalar

Finally, we consider a model with a complex color triplet scalar, s, with charge $Q = \frac{2}{3}$. It is interesting to see how the predictions differ from those of the T VLQ described above. The relevant interaction terms are,

$$L = m_0^2 s^{*A} s^A + \frac{\lambda_s}{2}(s^{*A} s^A)^2 + \kappa s^{*A} s^A \mid \phi^\dagger \phi \mid^2, \tag{A34}$$

where $A, B, C = 1...8$ are color indices. The mass of the colored scalar is $m_s^2 = m_0^2 + \frac{\kappa v^2}{2}$ and the parameter κ measures the amount of the scalar mass due to electroweak symmetry breaking. At tree level, the model generates 4 -fermion operators [6], $\mathcal{O}_{qq}^{(1)} = -\mathcal{O}_{qq}^{(3)}$ that do not contribute to our study, but enter at tree level in Drell-Yan and di-jet production at the LHC. At one loop, the colored scalar generates $\mathcal{O}_{HG}$,

$$\frac{C_{HG}}{\Lambda^2} = \frac{\alpha_s \kappa}{32\pi m_s^2} F_0(\tau_s) \to -\frac{\alpha_s \kappa}{96\pi m_s^2} \tag{A35}$$

where $F_0(\tau_s) = \tau_s \Big[1 - \tau_s f(\tau_s)\Big]$, $\tau_s = 4m_s^2/m_h^2$, and $f(\tau)$ is defined in Eq. A20.

[1] A. Biekotter, T. Corbett, and T. Plehn, "The Gauge-Higgs Legacy of the LHC Run II," *SciPost Phys.* **6** (2019) 064, arXiv:1812.07587 [hep-ph].

[2] C. Grojean, M. Montull, and M. Riembau, "Diboson at the LHC vs LEP," *JHEP* **03** (2019) 020, arXiv:1810.05149 [hep-ph].

[3] J. Ellis, C. W. Murphy, V. Sanz, and T. You, "Updated Global SMEFT Fit to Higgs, Diboson and Electroweak Data," *JHEP* **06** (2018) 146, arXiv:1803.03252 [hep-ph].

[4] E. da Silva Almeida, A. Alves, N. Rosa Agostinho, O. J. P. Éboli, and M. C. Gonzalez-Garcia, "Electroweak Sector Under Scrutiny: A Combined Analysis of LHC and Electroweak Precision Data," *Phys. Rev.* **D99** no. 3, (2019) 033001, arXiv:1812.01009 [hep-ph].

[5] S. Di Vita, C. Grojean, G. Panico, M. Riembau, and T. Vantalon, "A global view on the Higgs self-coupling," *JHEP* **09** (2017) 069, arXiv:1704.01953 [hep-ph].

[6] J. de Blas, J. Criado, M. Perez-Victoria, and J. Santiago, "Effective description of general extensions of the Standard Model: the complete tree-level dictionary," *JHEP* **03** (2018) 109, arXiv:1711.10391 [hep-ph].

[7] B. Henning, X. Lu, and H. Murayama, "How to use the Standard Model effective field theory," *JHEP* **01** (2016) 023, arXiv:1412.1837 [hep-ph].

[8] S. Das Bakshi, J. Chakrabortty, and S. K. Patra, "CoDEx: Wilson coefficient calculator connecting SMEFT to UV theory," *Eur. Phys. J. C* **79** no. 1, (2019) 21, arXiv:1808.04403 [hep-ph].

[9] C. Grojean, E. E. Jenkins, A. V. Manohar, and M. Trott, "Renormalization Group Scaling of Higgs Operators and $\Gamma(H \to \gamma\gamma)$," *JHEP* **04** (2013) 016, arXiv:1301.2588 [hep-ph].

[10] C.-Y. Chen, S. Dawson, and C. Zhang, "Electroweak Effective Operators and Higgs Physics," *Phys. Rev. D* **89** no. 1, (2014) 015016, arXiv:1311.3107 [hep-ph].

[11] J. de Blas *et al.*, "Higgs Boson Studies at Future Particle Colliders," *JHEP* **01** (2020) 139, arXiv:1905.03764 [hep-ph].

[12] R. S. Gupta, H. Rzehak, and J. D. Wells, "How well do we need to measure Higgs boson couplings?," *Phys. Rev. D* **86** (2012) 095001, arXiv:1206.3560 [hep-ph].

[13] J. Baglio, S. Dawson, S. Homiller, S. D. Lane, and I. M. Lewis, "Validity of SMEFT

studies of VH and VV Production at NLO," arXiv:2003.07862 [hep-ph].

[14] S. Dawson and P. P. Giardino, "Electroweak and QCD Corrections to Z and W pole observables in the SMEFT," arXiv:1909.02000 [hep-ph].

[15] M. Gorbahn, J. M. No, and V. Sanz, "Benchmarks for Higgs Effective Theory: Extended Higgs Sectors," *JHEP* **10** (2015) 036, arXiv:1502.07352 [hep-ph].

[16] M. Jiang, N. Craig, Y.-Y. Li, and D. Sutherland, "Complete One-Loop Matching for a Singlet Scalar in the Standard Model EFT," *JHEP* **02** (2019) 031, arXiv:1811.08878 [hep-ph].

[17] A. Dedes, W. Materkowska, M. Paraskevas, J. Rosiek, and K. Suxho, "Feynman Rules for the Standard Model Effective Field Theory in R_ξ-gauges," arXiv:1704.03888 [hep-ph].

[18] B. Grzadkowski, M. Iskrzynski, M. Misiak, and J. Rosiek, "Dimension-Six Terms in the Standard Model Lagrangian," *JHEP* **10** (2010) 085, arXiv:1008.4884 [hep-ph].

[19] A. Falkowski and D. Straub, "Flavourful SMEFT likelihood for Higgs and electroweak data," *JHEP* **04** (2020) 066, arXiv:1911.07866 [hep-ph].

[20] T. Corbett, O. Éboli, and M. Gonzalez-Garcia, "Unitarity Constraints on Dimension-six Operators II: Including Fermionic Operators," *Phys. Rev. D* **96** no. 3, (2017) 035006, arXiv:1705.09294 [hep-ph].

[21] A. Falkowski and F. Riva, "Model-independent precision constraints on dimension-6 operators," *JHEP* **02** (2015) 039, arXiv:1411.0669 [hep-ph].

[22] L. Berthier, M. Bjørn, and M. Trott, "Incorporating doubly resonant $W^\pm$ data in a global fit of SMEFT parameters to lift flat directions," *JHEP* **09** (2016) 157, arXiv:1606.06693 [hep-ph].

[23] G. Degrassi, P. Gambino, and P. P. Giardino, "The $m_W - m_Z$ interdependence in the Standard Model: a new scrutiny," *JHEP* **05** (2015) 154, arXiv:1411.7040 [hep-ph].

[24] G. D. Kribs, A. Maier, H. Rzehak, M. Spannowsky, and P. Waite, "Electroweak oblique parameters as a probe of the trilinear Higgs boson self-interaction," *Phys. Rev. D* **95** no. 9, (2017) 093004, arXiv:1702.07678 [hep-ph].

[25] G. Degrassi, P. P. Giardino, F. Maltoni, and D. Pagani, "Probing the Higgs self coupling via single Higgs production at the LHC," *JHEP* **12** (2016) 080, arXiv:1607.04251 [hep-ph].

[26] M. Gorbahn and U. Haisch, "Indirect probes of the trilinear Higgs coupling: $gg \to h$ and

$h \to \gamma\gamma$," *JHEP* **10** (2016) 094, arXiv:1607.03773 [hep-ph].

[27] W. Bizon, M. Gorbahn, U. Haisch, and G. Zanderighi, "Constraints on the trilinear Higgs coupling from vector boson fusion and associated Higgs production at the LHC," *JHEP* **07** (2017) 083, arXiv:1610.05771 [hep-ph].

[28] J. Baglio, S. Dawson, and I. M. Lewis, "NLO effects in EFT fits to W^+W^- production at the LHC," *Phys. Rev. D* **99** no. 3, (2019) 035029, arXiv:1812.00214 [hep-ph].

[29] E. E. Jenkins, A. V. Manohar, and M. Trott, "Renormalization Group Evolution of the Standard Model Dimension Six Operators I: Formalism and lambda Dependence," *JHEP* **10** (2013) 087, arXiv:1308.2627 [hep-ph].

[30] E. E. Jenkins, A. V. Manohar, and M. Trott, "Renormalization Group Evolution of the Standard Model Dimension Six Operators II: Yukawa Dependence," *JHEP* **01** (2014) 035, arXiv:1310.4838 [hep-ph].

[31] R. Alonso, E. E. Jenkins, A. V. Manohar, and M. Trott, "Renormalization Group Evolution of the Standard Model Dimension Six Operators III: Gauge Coupling Dependence and Phenomenology," *JHEP* **04** (2014) 159, arXiv:1312.2014 [hep-ph].

[32] S. Profumo, M. J. Ramsey-Musolf, C. L. Wainwright, and P. Winslow, "Singlet-catalyzed electroweak phase transitions and precision Higgs boson studies," *Phys. Rev. D* **91** no. 3, (2015) 035018, arXiv:1407.5342 [hep-ph].

[33] C.-Y. Chen, J. Kozaczuk, and I. M. Lewis, "Non-resonant Collider Signatures of a Singlet-Driven Electroweak Phase Transition," *JHEP* **08** (2017) 096, arXiv:1704.05844 [hep-ph].

[34] J. de Blas, M. Chala, M. Perez-Victoria, and J. Santiago, "Observable Effects of General New Scalar Particles," *JHEP* **04** (2015) 078, arXiv:1412.8480 [hep-ph].

[35] S. Dawson and C. W. Murphy, "Standard Model EFT and Extended Scalar Sectors," *Phys. Rev. D* **96** no. 1, (2017) 015041, arXiv:1704.07851 [hep-ph].

[36] C.-Y. Chen, S. Dawson, and I. Lewis, "Exploring resonant di-Higgs boson production in the Higgs singlet model," *Phys. Rev. D* **91** no. 3, (2015) 035015, arXiv:1410.5488 [hep-ph].

[37] J. F. Gunion and H. E. Haber, "The CP conserving two Higgs doublet model: The Approach to the decoupling limit," *Phys. Rev. D* **67** (2003) 075019, arXiv:hep-ph/0207010.

[38] J. Brehmer, A. Freitas, D. Lopez-Val, and T. Plehn, "Pushing Higgs Effective Theory to its Limits," *Phys. Rev. D* **93** no. 7, (2016) 075014, arXiv:1510.03443 [hep-ph].

[39] H. Belusca-Maito, A. Falkowski, D. Fontes, J. C. Romao, and J. P. Silva, "Higgs EFT for 2HDM and beyond," *Eur. Phys. J. C* **77** no. 3, (2017) 176, arXiv:1611.01112 [hep-ph].

[40] C.-Y. Chen, S. Dawson, and E. Furlan, "Vectorlike fermions and Higgs effective field theory revisited," *Phys. Rev. D* **96** no. 1, (2017) 015006, arXiv:1703.06134 [hep-ph].

[41] S. Dawson and E. Furlan, "A Higgs Conundrum with Vector Fermions," *Phys. Rev. D* **86** (2012) 015021, arXiv:1205.4733 [hep-ph].

[42] F. del Aguila, M. Perez-Victoria, and J. Santiago, "Effective description of quark mixing," *Phys. Lett. B* **492** (2000) 98–106, arXiv:hep-ph/0007160.

[43] C.-Y. Chen, S. Dawson, and I. Lewis, "Top Partners and Higgs Boson Production," *Phys. Rev. D* **90** no. 3, (2014) 035016, arXiv:1406.3349 [hep-ph].

[44] S. Dawson, A. Ismail, and I. Low, "What's in the loop? The anatomy of double Higgs production," *Phys. Rev. D* **91** no. 11, (2015) 115008, arXiv:1504.05596 [hep-ph].

[45] S. Dawson, I. Lewis, and M. Zeng, "Usefulness of effective field theory for boosted Higgs production," *Phys. Rev. D* **91** (2015) 074012, arXiv:1501.04103 [hep-ph].

[46] J. Baglio, S. Dawson, and S. Homiller, "QCD corrections in Standard Model EFT fits to WZ and WW production," *Phys. Rev. D* **100** no. 11, (2019) 113010, arXiv:1909.11576 [hep-ph].

[47] **ATLAS** Collaboration, G. Aad *et al.*, "Combined measurements of Higgs boson production and decay using up to 80 fb^{-1} of proton-proton collision data at $\sqrt{s} = 13$ TeV collected with the ATLAS experiment," *Phys. Rev. D* **101** no. 1, (2020) 012002, arXiv:1909.02845 [hep-ex].

[48] **CMS** Collaboration, "Combined Higgs boson production and decay measurements with up to 137 fb^{-1} of proton-proton collision data at $\sqrt{s} = 13$ TeV,". https://cds.cern.ch/record/2706103.

[49] **ATLAS** Collaboration, "Methodology for EFT interpretation of Higgs boson Simplified Template Cross-section results in ATLAS,". https://cds.cern.ch/record/2694284.

[50] J. D. Wells and Z. Zhang, "Renormalization group evolution of the universal theories EFT," *JHEP* **06** (2016) 122, arXiv:1512.03056 [hep-ph].

[51] M. Capozi and G. Heinrich, "Exploring anomalous couplings in Higgs boson pair

production through shape analysis," *JHEP* **03** (2020) 091, arXiv:1908.08923 [hep-ph].

[52] T. Robens and T. Stefaniak, "Status of the Higgs Singlet Extension of the Standard Model after LHC Run 1," *Eur. Phys. J. C* **75** (2015) 104, arXiv:1501.02234 [hep-ph].

[53] A. Falkowski, C. Gross, and O. Lebedev, "A second Higgs from the Higgs portal," *JHEP* **05** (2015) 057, arXiv:1502.01361 [hep-ph].

[54] D. Lopez-Val and T. Robens, "Δr and the W-boson mass in the singlet extension of the standard model," *Phys. Rev. D* **90** (2014) 114018, arXiv:1406.1043 [hep-ph].

[55] S. Dawson and W. Yan, "Hiding the Higgs Boson with Multiple Scalars," *Phys. Rev. D* **79** (2009) 095002, arXiv:0904.2005 [hep-ph].

[56] H. E. Haber and O. Stål, "New LHC benchmarks for the $\mathcal{CP}$ -conserving two-Higgs-doublet model," *Eur. Phys. J. C* **75** no. 10, (2015) 491, arXiv:1507.04281 [hep-ph]. [Erratum: Eur.Phys.J.C 76, 312 (2016)].

[57] F. Bishara, U. Haisch, P. F. Monni, and E. Re, "Constraining Light-Quark Yukawa Couplings from Higgs Distributions," *Phys. Rev. Lett.* **118** no. 12, (2017) 121801, arXiv:1606.09253 [hep-ph].

[58] L. Alasfar, R. Corral Lopez, and R. Grober, "Probing Higgs couplings to light quarks via Higgs pair production," *JHEP* **11** (2019) 088, arXiv:1909.05279 [hep-ph].

[59] D. Egana-Ugrinovic, S. Homiller, and P. R. Meade, "Higgs bosons with large couplings to light quarks," *Phys. Rev. D* **100** no. 11, (2019) 115041, arXiv:1908.11376 [hep-ph].

[60] S. L. Glashow and S. Weinberg, "Natural Conservation Laws for Neutral Currents," *Phys. Rev. D* **15** (1977) 1958.

[61] J. Brehmer, S. Dawson, S. Homiller, F. Kling, and T. Plehn, "Benchmarking simplified template cross sections in WH production," *JHEP* **11** (2019) 034, arXiv:1908.06980 [hep-ph].

[62] T. Barklow, K. Fujii, S. Jung, R. Karl, J. List, T. Ogawa, M. E. Peskin, and J. Tian, "Improved Formalism for Precision Higgs Coupling Fits," *Phys. Rev. D* **97** no. 5, (2018) 053003, arXiv:1708.08912 [hep-ph].

[63] G. Durieux and O. Matsedonskyi, "The top-quark window on compositeness at future lepton colliders," *JHEP* **01** (2019) 072, arXiv:1807.10273 [hep-ph].

[64] A. Buckley, C. Englert, J. Ferrando, D. J. Miller, L. Moore, M. Russell, and C. D. White, "Constraining top quark effective theory in the LHC Run II era," *JHEP* **04** (2016) 015,

arXiv:1512.03360 [hep-ph].

[65] V. Cirigliano, W. Dekens, J. de Vries, and E. Mereghetti, "Constraining the top-Higgs sector of the Standard Model Effective Field Theory," *Phys. Rev. D* **94** no. 3, (2016) 034031, arXiv:1605.04311 [hep-ph].

[66] N. P. Hartland, F. Maltoni, E. R. Nocera, J. Rojo, E. Slade, E. Vryonidou, and C. Zhang, "A Monte Carlo global analysis of the Standard Model Effective Field Theory: the top quark sector," *JHEP* **04** (2019) 100, arXiv:1901.05965 [hep-ph].

[67] G. Durieux, A. Irles, V. Miralles, A. Penuelas, R. Poschl, M. Perello, and M. Vos, "The electro-weak couplings of the top and bottom quarks – global fit and future prospects," *JHEP* **12** (2019) 098, arXiv:1907.10619 [hep-ph].

[68] I. Brivio, S. Bruggisser, F. Maltoni, R. Moutafis, T. Plehn, E. Vryonidou, S. Westhoff, and C. Zhang, "O new physics, where art thou? A global search in the top sector," *JHEP* **02** (2020) 131, arXiv:1910.03606 [hep-ph].

[69] S. A. R. Ellis, J. Quevillon, T. You, and Z. Zhang, "Extending the Universal One-Loop Effective Action: Heavy-Light Coefficients," *JHEP* **08** (2017) 054, arXiv:1706.07765 [hep-ph].

[70] U. Haisch, M. Ruhdorfer, E. Salvioni, E. Venturini, and A. Weiler, "Singlet night in Feynman-ville: one-loop matching of a real scalar," *JHEP* **04** (2020) 164, arXiv:2003.05936 [hep-ph]. [Erratum: JHEP 07, 066 (2020)].

[71] F. del Aguila, Z. Kunszt, and J. Santiago, "One-loop effective lagrangians after matching," *Eur. Phys. J. C* **76** no. 5, (2016) 244, arXiv:1602.00126 [hep-ph].

[72] A. Angelescu and P. Huang, "Integrating Out New Fermions at One Loop," arXiv:2006.16532 [hep-ph].

[73] L. Alasfar, A. Azatov, J. de Blas, A. Paul, and M. Valli, "B anomalies under the lens of electroweak precision," arXiv:2007.04400 [hep-ph].

[74] S. Descotes-Genon, A. Falkowski, M. Fedele, M. Gonzalez-Alonso, and J. Virto, "The CKM parameters in the SMEFT," *JHEP* **05** (2019) 172, arXiv:1812.08163 [hep-ph].

[75] R. Aoude, T. Hurth, S. Renner, and W. Shepherd, "The impact of flavour data on global fits of the MFV SMEFT," arXiv:2003.05432 [hep-ph].

[76] J. Aebischer and J. Kumar, "Flavour Violating Effects of Yukawa Running in SMEFT," arXiv:2005.12283 [hep-ph].

[77] C. Bobeth, A. J. Buras, A. Celis, and M. Jung, "Patterns of Flavour Violation in Models with Vector-Like Quarks," *JHEP* **04** (2017) 079, arXiv:1609.04783 [hep-ph].

[78] T. Corbett, A. Joglekar, H.-L. Li, and J.-H. Yu, "Exploring Extended Scalar Sectors with Di-Higgs Signals: A Higgs EFT Perspective," *JHEP* **05** (2018) 061, arXiv:1705.02551 [hep-ph].

[79] S. Davidson and H. E. Haber, "Basis-independent methods for the two-Higgs-doublet model," *Phys. Rev. D* **72** (2005) 035004, arXiv:hep-ph/0504050. [Erratum: Phys.Rev.D 72, 099902 (2005)].

[80] L. Lavoura and J. P. Silva, "The Oblique corrections from vector - like singlet and doublet quarks," *Phys. Rev. D* **47** (1993) 2046–2057.

[81] J. Aguilar-Saavedra, R. Benbrik, S. Heinemeyer, and M. Perez-Victoria, "Handbook of vectorlike quarks: Mixing and single production," *Phys. Rev. D* **88** no. 9, (2013) 094010, arXiv:1306.0572 [hep-ph].

[82] G. Cacciapaglia, A. Deandrea, D. Harada, and Y. Okada, "Bounds and Decays of New Heavy Vector-like Top Partners," *JHEP* **11** (2010) 159, arXiv:1007.2933 [hep-ph].

[83] **ALEPH, DELPHI, L3, OPAL, SLD, LEP Electroweak Working Group, SLD Electroweak Group, SLD Heavy Flavour Group** Collaboration, S. Schael *et al.*, "Precision electroweak measurements on the Z resonance," *Phys. Rept.* **427** (2006) 257–454, arXiv:hep-ex/0509008.